A Complex Weighted Discounting Multisource Information Fusion with its Application in Pattern Classification

Fuyuan Xiao, *Senior Member, IEEE*, Zehong Cao, *Member, IEEE*, Chin-Teng Lin, *Fellow, IEEE*

Abstract—Complex evidence theory (CET) is an effective method for uncertainty reasoning in knowledge-based systems with good interpretability that has recently attracted much attention. However, approaches to improve the performance of uncertainty reasoning in CET-based expert systems remains an open issue. One key to performance improvement is the adequate management of conflict from multisource information. In this paper, a generalized correlation coefficient, namely, the complex evidential correlation coefficient (CECC), is proposed for the complex mass functions or complex basic belief assignments (CBBAs) in CET. On this basis, a complex conflict coefficient is proposed to measure the conflict between CBBAs; when CBBAs turn into classic BBAs, the complex correlation and conflict coefficients will degrade into traditional coefficients. The complex conflict coefficient satisfies nonnegativity, symmetry, boundedness, extreme consistency, and insensitivity to refinement properties, which are desirable for conflict measurement. Several numerical examples validate through comparisons the superiority of the complex conflict coefficient. In this context, a weighted discounting multisource information fusion algorithm, which is called the CECC-WDMSIF, is designed based on the CECC to improve the performance of CET-based expert systems. By applying the CECC-WDMSIF method to the pattern classification of diverse real-world datasets, it is demonstrated that the proposed CECC-WDMSIF outperforms well-known related approaches with higher classification accuracy and robustness.

Index Terms—Uncertainty reasoning, Complex evidence theory, Complex mass function, Complex evidential correlation coefficient, Conflict management, Pattern classification, Expert system.

1 Introduction

The issue of approaching uncertainty reasoning in knowledge-based systems with an interpretable manner has attracted much attention [1–3]. To date, various methods have been presented, such as extended fuzzy sets [4], evidence theory [5], Z numbers [6], and others, which are broadly used in uncertain expert systems [7]. Among these methods, Dempster–Shafer evidence (DSE) theory [8, 9] has several satisfying traits for handling uncertainty in expert systems, and it is applied in a number of fields of data engineering, such as reliability evaluation [10], network community detection [11, 12], metro systems control [13], clustering [14], and classification [15]. Evidence theory can quantitatively represent uncertainty [16], while Dempster's combination rule (DCR) follows the commutative and associative laws [17]. In addition, the fused result of DCR is fault-tolerant, and uncertainty can also be decreased after DCR. As a result, DSE theory can better support decision making [18]; therefore, this theory has been well investigated and extended in studies on evidential reasoning [19, 20], belief rule-based systems [21], evidence reliability evaluation [22], etc.

Corresponding author: Fuyuan Xiao.
F. Xiao is with the School of Big Data and Software Engineering, Chongqing University, Chongqing 401331, China. (e-mail: xiaofuyuan@cqu.edu.cn.)
Z. Cao is with the STEM, Mawson Lakes Campus, University of South Australia, Adelaide, SA 5095, Australia (email: zhccaonctu@gmail.com).
C.-T. Lin is with the Center for Artificial Intelligence, Faculty of Engineering and IT, University of Technology Sydney, Sydney, NSW, Australia (email: Chin-Teng.Lin@uts.edu.au).

It is well known that the complex-valued model has stronger presentational capabilities [23, 24]; for example, its novelty is manifested in the phase of the grade of membership with the physical meaning as a manner of expressing cyclical phenomena, which is significant in incorporating more information. Various traditional theories have been generalized, such as complex fuzzy sets [23], complex intuitionistic fuzzy sets [25], and complex Pythagorean fuzzy sets [26], including the following applications: pattern recognition [26, 27], quantum information fusion [28], and parrondo effects [29]. Therefore, in recent work on complex evidence theory (CET) proposed by Xiao [30, 31], the new concepts of complex mass functions (CMFs) or CBBAs are defined on the basis of the complex plane. Naturally, the complex-value-modeled CET [30, 31] inherits the advantages of traditional evidence theory. In addition, due to the superiority of CBBAs with the additional dimension of the phase of complex mass function, CET can similarly express data fluctuations at a given time phase, and handle uncertainty when an event occurs simultaneously with changes in the periodicity of the data [25]. In particular, when CBBAs are without phase terms and turn into classic BBAs, CET degrades to DSE theory under the condition with the conflict coefficient $|\mathbb{K}|$ less than 1 (Details will be illustrated in Section 2). Therefore, CET provides a more promising approach to uncertainty reasoning in expert systems than that in DSE [28].

In real-world applications of data engineering, conflicting information is inevitable. Accordingly, conflict management in evidence theory-based expert systems plays an

important role in the performance of uncertainty reasoning. In traditional DSE theory, it is well known that the conflict coefficient k [8, 9] combines the mass assigned to the empty set. k takes into account the conflict among focal elements while ignoring the global consistency among different pieces of evidence. To address this issue, lots of studies put forward potential solutions from different perspectives. For instance, some work presented different kinds of distance functions [32–34]; some researchers came up with information quality [35]; other methods, such as entropy [36] and divergence measures [37, 38], have been introduced to quantify the consistency of the evidence; other conflict management methods based on ordered visibility graph [39], networks [40], and autoencoder-K-means [41] are also presented; another study also discussed the conflict measure viewed from correlation coefficients [42]. In addition to CET theory, several research focus on conflict management based on distance. For example, Xiao [43] generalized Jousselme et al.'s [32] distance measure for complex mass functions. Although the abovementioned conflict measures are effective for classic DSE theory-based expert systems, they are difficult to handle the conflict problem in CET-based expert systems. In summary, the conflict management in CET is still in an early research stage with various challenges.

In this paper, we address this problem from the perspective of correlation coefficient, where a complex evidential correlation coefficient (CECC) is proposed that measures the correlation coefficient between CBBAs for conflict management in CET-based expert systems. On the basis of the CECC, a complex conflict coefficient is then presented to measure the conflict between CBBAs. We next analyze and prove that the complex conflict coefficient has satisfying nonnegativity, symmetry, boundedness, extreme consistency, and insensitivity to refinement properties for conflict measurement. In particular, when CBBAs turn into classic BBAs, the correlation and conflict coefficients degrade into traditional coefficients. The complex conflict coefficient is also compared with related works, and the results validate the proposed method's superiority. Moreover, a weighted discounting multisource information fusion algorithm, which is called the CECC-WDMSIF, is designed based on the CECC to improve the performance of CET-based expert systems. By applying the CECC-WDMSIF method to the pattern classification of real-world datasets, we demonstrate that the proposed CECC-WDMSIF has advantages for diverse datasets and outperforms well-known related works with higher classification accuracy and robustness.

The main contributions are summarized below.

- This is the first work to study the correlation and conflict coefficients between complex mass functions in CET. This work proves that the complex conflict coefficient has satisfying nonnegativity, symmetry, boundedness, extreme consistency, and insensitivity to refinement properties, which are desirable for conflict measurement in CET.
- On the basis of the CECC, a weighted discounting multisource information fusion algorithm, which is called the CECC-WDMSIF, is first designed to improve the performance of CET-based expert systems. Through a weighted discounting process for complex evidence, the CECC-WDMSIF can well handle the influence of conflicting data on CET-based expert systems to improve the decision level with a better robustness.
- To demonstrate the effectiveness of the proposed CECC-WDMSIF, it is applied to the pattern classification of real-world datasets to validate its practicability and superiority. The experimental results illustrate that the outcomes of the proposed CECC-WDMSIF offer the highest classification accuracy and robustness on diverse real-world datasets compared to eleven well-known related methods.

The rest of this paper is organized as follows: The CET is introduced in Section 2. The CECC and conflict coefficient between CBBAs are proposed in Section 3. Section 4 compares the proposed complex conflict coefficient with related works to demonstrate its superiority. In Section 5, a weighted discounting multisource information fusion algorithm is designed based on the CECC. In Section 6, the CECC-WDMSIF algorithm is applied to pattern classification to validate its practicability and superiority. Finally, Section 7 concludes this work.

2 Complex Evidence Theory

To handle uncertainty problems in expert systems, many methods have been presented [44–47]. Among them, CET [30, 31] is a useful method that is briefly introduced below.

Definition 1 *(Frame of discernment) Let $\mathbf{\Omega}$ be a set of mutually exclusive and collective nonempty events. The frame of discernment (FOD) is defined by $\mathbf{\Omega} = \{C_1, C_2, \ldots, C_p, \ldots, C_n\}$.*

Definition 2 *(Hypothesis) The power set of $\mathbf{\Omega}$ is denoted by*

$$2^{\mathbf{\Omega}} = \{\emptyset, \{C_1\}, \{C_2\}, \ldots, \{C_n\}, \{C_1, C_2\}, \ldots, \{C_1, C_2, \ldots, C_n\}, \ldots, \mathbf{\Omega}\}, \tag{1}$$

and $\emptyset$ is an empty set. $\mathcal{A}_j \in 2^{\mathbf{\Omega}}$ is defined as a proposition or hypothesis.

Definition 3 *(Complex mass function) A CMF $\mathbb{M}$ in FOD $\mathbf{\Omega}$ is modeled by a complex number, which is represented as a mapping:*

$$\mathbb{M}: \quad 2^{\mathbf{\Omega}} \to \mathbb{C}, \tag{2}$$

which satisfies

$$\begin{aligned} &\mathbb{M}(\emptyset) = 0, \\ &\mathbb{M}(\mathcal{A}_j) = \mathbf{m}(\mathcal{A}_j) e^{i\theta(\mathcal{A}_j)}, \quad \mathcal{A}_j \subseteq \mathbf{\Omega} \\ &\sum_{\mathcal{A}_j \in 2^{\mathbf{\Omega}}} \mathbb{M}(\mathcal{A}_j) = 1, \end{aligned} \tag{3}$$

where $i = \sqrt{-1}$; $\mathbf{m}(\mathcal{A}_j) \in [0, 1]$ represents the magnitude of $\mathbb{M}(\mathcal{A}_j)$, and $\theta(\mathcal{A}_j)$ represents a phase of $\mathbb{M}(\mathcal{A}_j)$.

CMF $\mathbb{M}$ is also called a CBBA or complex evidence and is a generalized model of a classic basic belief assignment (BBA) in DSE theory. Since a BBA can effectively model uncertainty, its operations have been well studied, such as probability transformation [39], information fractal dimension [48] and information volume [49, 50].

In Eq. (3), $\mathbb{M}(\mathcal{A}_j)$ is also expressed in another form:

$$\mathbb{M}(\mathcal{A}_j) = x + yi, \quad \mathcal{A}_j \in 2^{\mathbf{\Omega}} \tag{4}$$

with

$$\sqrt{x^2+y^2} \in [0,1]. \tag{5}$$

Then, it can be deduced that

$$\mathbf{m}(\mathcal{A}_j) = \sqrt{x^2+y^2}, \text{ and } \theta(\mathcal{A}_j) = \arctan\left(\frac{y}{x}\right), \tag{6}$$

in which $x = \mathbf{m}(\mathcal{A}_j)\cos(\theta(\mathcal{A}_j))$ and $y = \mathbf{m}(\mathcal{A}_j)\sin(\theta(\mathcal{A}_j))$.

In addition,

$$|\mathbb{M}(\mathcal{A}_j)|^2 = \mathbb{M}(\mathcal{A}_j)\widehat{\mathbb{M}}(\mathcal{A}_j) = x^2 + y^2, \tag{7}$$

where $\widehat{\mathbb{M}}(\mathcal{A}_j) = x - yi$ is the complex conjugate of $\mathbb{M}(\mathcal{A}_j)$.

Therefore,

$$\mathbf{m}(\mathcal{A}_j) = |\mathbb{M}(\mathcal{A})|, \text{ and } \theta(\mathcal{A}_j) = \angle\mathbb{M}(\mathcal{A}_j), \tag{8}$$

in which when $\mathbb{M}(\mathcal{A}_j)$ is a positive real number, $\mathbb{M}(\mathcal{A}_j) = \mathbf{m}(\mathcal{A}_j) = |x|$.

For $\mathcal{A}_j \in 2^{\mathbf{\Omega}}$, when $|\mathbb{M}(\mathcal{A}_j)| > 0$, $\mathcal{A}_j$ is called a focal element of $\mathbb{M}$. The value of $|\mathbb{M}(\mathcal{A}_j)|$ expresses the support degree for $\mathcal{A}_j$.

Definition 4 *(Complex evidence combination rule) Let $\mathbb{M}_h$ and $\mathbb{M}_k$ be two independent CBBAs in FOD $\mathbf{\Omega}$. The CECR, which is denoted as $\mathbb{M} = \mathbb{M}_h \oplus \mathbb{M}_k$, is defined by*

$$\mathbb{M}(\mathcal{A}) = \begin{cases} \frac{1}{1-\mathbb{K}} \sum\limits_{\mathcal{A}_i \cap \mathcal{A}_j = \mathcal{A}} \mathbb{M}_h(\mathcal{A}_i)\mathbb{M}_k(\mathcal{A}_j), & \mathcal{A} \neq \emptyset, \\ 0, & \mathcal{A} = \emptyset, \end{cases} \tag{9}$$

with

$$\mathbb{K} = \sum_{\mathcal{A}_i \cap \mathcal{A}_j = \emptyset} \mathbb{M}_h(\mathcal{A}_i)\mathbb{M}_k(\mathcal{A}_j), \tag{10}$$

where $\mathcal{A}_i, \mathcal{A}_j \in 2^{\mathbf{\Omega}}$, and $\mathbb{K}$ is the conflict coefficient between $\mathbb{M}_h$ and $\mathbb{M}_k$. Note that the CECR is only feasible when $\mathbb{K} \neq 1$.

3 The Correlation and Conflict Coefficients for Complex Mass Functions

In this section, a CECC is first proposed to measure the correlation coefficients among CBBAs, as inspired by [42]. Additionally, the properties of the CECC are analyzed and proven. Based on the CECC, a complex conflict coefficient is then defined. We find that the complex conflict coefficient has satisfying nonnegativity, symmetry, boundedness, extreme consistency, and insensitivity to refinement properties for conflict measurement.

Definition 5 *(CECC between CBBAs) Let $\mathbb{M}_h$ and $\mathbb{M}_k$ be two CBBAs on FOD $\mathbf{\Omega}$, where $\mathcal{A}_i$ and $\mathcal{A}_j$ are the hypotheses of $\mathbb{M}_h$ and $\mathbb{M}_k$, respectively; $\widehat{\mathbb{M}}_h(\mathcal{A}_i)$ and $\widehat{\mathbb{M}}_k(\mathcal{A}_j)$ are complex conjugates of $\mathbb{M}_h(\mathcal{A}_i)$ and $\mathbb{M}_k(\mathcal{A}_j)$, respectively. The CECC between CBBAs $\mathbb{M}_h$ and $\mathbb{M}_k$, which is denoted as $\mathbb{C}(\overrightarrow{\mathbb{M}}_h, \overrightarrow{\mathbb{M}}_k)$, is defined by*

$$\mathbb{C}(\overrightarrow{\mathbb{M}}_h, \overrightarrow{\mathbb{M}}_k) = \frac{\sqrt{\langle \overrightarrow{\mathbb{M}}_h, \overrightarrow{\mathbb{M}}_k \rangle \langle \overrightarrow{\mathbb{M}}_k, \overrightarrow{\mathbb{M}}_h \rangle}}{\|\overrightarrow{\mathbb{M}}_h\| \|\overrightarrow{\mathbb{M}}_k\|}, \tag{11}$$

where $\langle \cdot \rangle$ is the inner product

$$\langle \overrightarrow{\mathbb{M}}_h, \overrightarrow{\mathbb{M}}_k \rangle = \overrightarrow{\mathbb{M}}_h \cdot \overrightarrow{\mathbb{M}}_k = \sum_{i=1}^{2^n-1} \sum_{j=1}^{2^n-1} \mathbb{M}_h(\mathcal{A}_i)\widehat{\mathbb{M}}_k(\mathcal{A}_j) \frac{|\mathcal{A}_i \cap \mathcal{A}_j|}{|\mathcal{A}_i \cup \mathcal{A}_j|},$$

$$\langle \overrightarrow{\mathbb{M}}_k, \overrightarrow{\mathbb{M}}_h \rangle = \overrightarrow{\mathbb{M}}_k \cdot \overrightarrow{\mathbb{M}}_h = \sum_{j=1}^{2^n-1} \sum_{i=1}^{2^n-1} \mathbb{M}_k(\mathcal{A}_j)\widehat{\mathbb{M}}_h(\mathcal{A}_i) \frac{|\mathcal{A}_j \cap \mathcal{A}_i|}{|\mathcal{A}_j \cup \mathcal{A}_i|};$$

$\|\cdot\|$ is the norm of the CBBA

$$\|\overrightarrow{\mathbb{M}}\|^2 = \langle \overrightarrow{\mathbb{M}}, \overrightarrow{\mathbb{M}} \rangle = \sum_{i=1}^{2^n-1} \sum_{j=1}^{2^n-1} \mathbb{M}(\mathcal{A}_i)\widehat{\mathbb{M}}(\mathcal{A}_j) \frac{|\mathcal{A}_i \cap \mathcal{A}_j|}{|\mathcal{A}_i \cup \mathcal{A}_j|}.$$

For Eq. (11), since CBBAs $\mathbb{M}_h$ and $\mathbb{M}_k$ are complex-valued, we can learn that

$$\langle \overrightarrow{\mathbb{M}}_h, \overrightarrow{\mathbb{M}}_k \rangle \neq \langle \overrightarrow{\mathbb{M}}_k, \overrightarrow{\mathbb{M}}_h \rangle. \tag{12}$$

When the belief values of CBBAs $\mathbb{M}_h$ and $\mathbb{M}_k$ convert into positive real numbers from complex numbers, we have $\mathbb{M}(\mathcal{A}) = \mathbf{m}(\mathcal{A}) = x$, while $y = 0$, such that

$$\begin{aligned} \langle \overrightarrow{\mathbb{M}}_h, \overrightarrow{\mathbb{M}}_k \rangle = \langle \overrightarrow{\mathbb{M}}_k, \overrightarrow{\mathbb{M}}_h \rangle &= \sum_{i=1}^{2^n-1} \sum_{j=1}^{2^n-1} \mathbf{m}_h(\mathcal{A}_i)\mathbf{m}_k(\mathcal{A}_j) \frac{|\mathcal{A}_i \cap \mathcal{A}_j|}{|\mathcal{A}_i \cup \mathcal{A}_j|} \\ &= \langle \overrightarrow{\mathbf{m}}_h, \overrightarrow{\mathbf{m}}_k \rangle. \end{aligned} \tag{13}$$

In this case, because

$$\|\overrightarrow{\mathbb{M}}\|^2 = \sum_{i=1}^{2^n-1} \sum_{j=1}^{2^n-1} \mathbf{m}(\mathcal{A}_i)\mathbf{m}(\mathcal{A}_j) \frac{|\mathcal{A}_i \cap \mathcal{A}_j|}{|\mathcal{A}_i \cup \mathcal{A}_j|} = \|\overrightarrow{\mathbf{m}}\|, \tag{14}$$

$\mathbb{C}(\overrightarrow{\mathbb{M}}_h, \overrightarrow{\mathbb{M}}_k)$ can then be expressed in the following form:

$$\mathbb{C}(\overrightarrow{\mathbb{M}}_h, \overrightarrow{\mathbb{M}}_k) = \frac{\langle \overrightarrow{\mathbb{M}}_h, \overrightarrow{\mathbb{M}}_k \rangle}{\|\overrightarrow{\mathbb{M}}_h\| \|\overrightarrow{\mathbb{M}}_k\|} = \frac{\langle \overrightarrow{\mathbf{m}}_h, \overrightarrow{\mathbf{m}}_k \rangle}{\|\overrightarrow{\mathbf{m}}_h\| \|\overrightarrow{\mathbf{m}}_k\|}. \tag{15}$$

From Eq. (15), it is obvious that when CBBAs are degraded from complex numbers into positive real numbers, the CECC degrades into Jiang's correlation coefficient [42].

Property 1 *The CECC is a generalization of the classic correlation coefficient, i.e., that of Jiang [42].*

Theorem 1 *The CECC has nonnegativity, nondegeneracy, symmetry and boundedness properties.*

Property 2 *Let $\mathbb{M}_h$, $\mathbb{M}_k$ and $\mathbb{M}_3$ be three arbitrary CBBAs:*

P 2.1 Nonnegativity: $\mathbb{C}(\mathbb{M}_h, \mathbb{M}_k) \geq 0$.

P 2.2 Nondegeneracy: $\mathbb{C}(\mathbb{M}_h, \mathbb{M}_k) = 1$ iff $\mathbb{M}_h = \mathbb{M}_k$.

P 2.3 Symmetry: $\mathbb{C}(\mathbb{M}_h, \mathbb{M}_k) = \mathbb{C}(\mathbb{M}_k, \mathbb{M}_h)$.

P 2.4 Boundedness: $0 \leq \mathbb{C}(\mathbb{M}_h, \mathbb{M}_k) \leq 1$.

The proofs are provided in the Appendix.

Next, several numerical examples illustrate the CECC's properties.

Example 1 Consider two CBBAs, $\mathbb{M}_h$ and $\mathbb{M}_k$, in FOD $\mathbf{\Omega} = \{\mathcal{A}_1, \mathcal{A}_2\}$:

$$\begin{aligned} \mathbb{M}_h : &\mathbb{M}_h(\{\mathcal{A}_1\}) = 0.7280e^{i\arctan(-0.2857)}, \\ &\mathbb{M}_h(\{\mathcal{A}_2\}) = 0.1803e^{i\arctan(0.6667)}, \\ &\mathbb{M}_h(\{\mathcal{A}_1, \mathcal{A}_2\}) = 0.1803e^{i\arctan(0.6667)}; \\ \mathbb{M}_k : &\mathbb{M}_k(\{\mathcal{A}_1\}) = 0.7280e^{i\arctan(-0.2857)}, \\ &\mathbb{M}_k(\{\mathcal{A}_2\}) = 0.1803e^{i\arctan(0.6667)}, \\ &\mathbb{M}_k(\{\mathcal{A}_1, \mathcal{A}_2\}) = 0.1803e^{i\arctan(0.6667)}. \end{aligned}$$

From Example 1, we can see that $\mathbb{M}_h$ and $\mathbb{M}_k$ have the same CBBAs, where $\mathbb{M}_h(\{\mathcal{A}_1\}) = \mathbb{M}_k(\{\mathcal{A}_1\}) = 0.7280e^{i\arctan(-0.2857)}$, $\mathbb{M}_h(\{\mathcal{A}_2\}) = \mathbb{M}_k(\{\mathcal{A}_2\}) = 0.1803e^{i\arctan(0.6667)}$, and $\mathbb{M}_h(\{\mathcal{A}_1, \mathcal{A}_2\}) =$

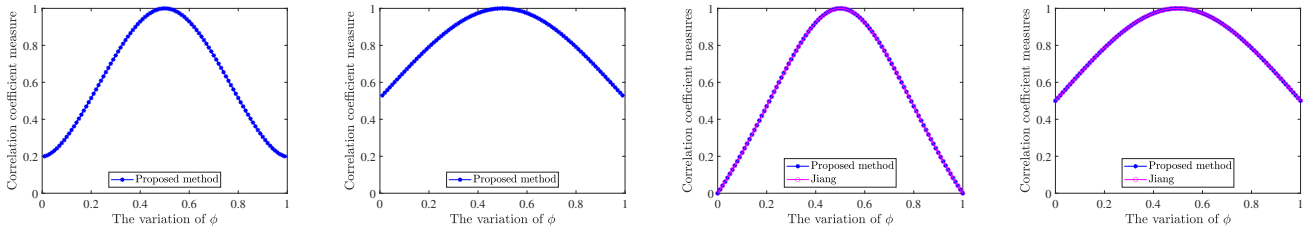

(a) $\psi = 0.1$ and $\omega = \{\mathcal{A}_2\}$. (b) $\psi = 0.1$ and $\omega = \{\mathcal{A}_1, \mathcal{A}_2\}$. (c) $\psi = 0$ and $\omega = \{\mathcal{A}_2\}$. (d) $\psi = 0$ and $\omega = \{\mathcal{A}_1, \mathcal{A}_2\}$.

Fig. 1. Comparisons of different correlation coefficient measures under the value and subset variations of focal elements in Example 3.

$\mathbb{M}_k(\{\mathcal{A}_1, \mathcal{A}_2\}) = 0.1803e^{i\arctan(0.6667)}$. Additionally, $|\mathbb{M}_h|$ and $|\mathbb{M}_k|$ have the same value of 0.7280 to support $\mathcal{A}_1$.

Next, we calculate the CECC between $\mathbb{M}_h$ and $\mathbb{M}_k$:

$$\mathbb{C}(\mathbb{M}_h, \mathbb{M}_k) = 1.$$

This result shows that when $\mathbb{M}_h$ and $\mathbb{M}_k$ are the same, the CECC measure is one, which demonstrates the expected behavior.

Example 2 Consider two CBBAs, $\mathbb{M}_h$ and $\mathbb{M}_k$, in FOD $\mathbf{\Omega} = \{\mathcal{A}_1, \mathcal{A}_2\}$:

$$\begin{aligned}
\mathbb{M}_h :& \mathbb{M}_h(\{\mathcal{A}_1\}) = 0.7280e^{i\arctan(-0.2857)},\\
& \mathbb{M}_h(\{\mathcal{A}_2\}) = 0.1803e^{i\arctan(0.6667)},\\
& \mathbb{M}_h(\{\mathcal{A}_1, \mathcal{A}_2\}) = 0.1803e^{i\arctan(0.6667)};\\
\mathbb{M}_k :& \mathbb{M}_k(\{\mathcal{A}_1\}) = 0.1414e^{i\arctan(1.0000)},\\
& \mathbb{M}_k(\{\mathcal{A}_2\}) = 0.7762e^{i\arctan(-0.2667)},\\
& \mathbb{M}_k(\{\mathcal{A}_1, \mathcal{A}_2\}) = 0.1803e^{i\arctan(0.6667)}.
\end{aligned}$$

In Example 2, it is obvious that $\mathbb{M}_h$ and $\mathbb{M}_k$ have different CBBAs, where $\mathbb{M}_h(\{\mathcal{A}_1\}) = 0.7280e^{i\arctan(-0.2857)}$ and $\mathbb{M}_k(\{\mathcal{A}_1\}) = 0.1803e^{i\arctan(0.6667)}$; $\mathbb{M}_h(\{\mathcal{A}_2\}) = 0.1803e^{i\arctan(0.6667)}$ and $\mathbb{M}_k(\{\mathcal{A}_2\}) = 0.7762e^{i\arctan(-0.2667)}$; and $\mathbb{M}_h(\{\mathcal{A}_1, \mathcal{A}_2\}) = 0.1414e^{i\arctan(1.0000)}$ and $\mathbb{M}_k(\{\mathcal{A}_1, \mathcal{A}_2\}) = 0.1803e^{i\arctan(0.6667)}$.

Additionally, $|\mathbb{M}_h|$ is 0.7280 to support $\mathcal{A}_1$, while $|\mathbb{M}_k|$ is 0.7762 to support $\mathcal{A}_2$.

Then, we calculate the following:

$$\mathbb{C}(\mathbb{M}_h, \mathbb{M}_k) = 0.3948.$$

This result describes the CECC's expected behavior. When two CBBAs are not equal to one another, the CECC measure is greater than zero.

Furthermore, we calculate the CECC between $\mathbb{M}_k$ and $\mathbb{M}_h$:

$$\mathbb{C}(\mathbb{M}_k, \mathbb{M}_h) = 0.3948.$$

It is obvious that $\mathbb{C}(\mathbb{M}_h, \mathbb{M}_k) = \mathbb{C}(\mathbb{M}_k, \mathbb{M}_h)$, which verifies the symmetry property of the CECC.

Example 3 Consider the two CBBAs of $\mathbb{M}_h$ and $\mathbb{M}_k$ in FOD $\mathbf{\Omega}$:

$$\begin{aligned}
\mathbb{M}_h :&\quad \mathbb{M}_h(\{\mathcal{A}_1\}) = \phi + \psi i, \mathbb{M}_h(\omega) = 1 - \phi - \psi i;\\
\mathbb{M}_k :&\quad \mathbb{M}_k(\{\mathcal{A}_1\}) = 1 - \phi + \psi i, \mathbb{M}_k(\omega) = \phi - \psi i.
\end{aligned}$$

In Example 3, $\mathbb{M}_h$ and $\mathbb{M}_k$ vary in accordance with ϕ and ω. In this example, $\phi \in [0, 1]$ and $\psi = 0.1$. ω is $\{\mathcal{A}_2\}$ or $\{\mathcal{A}_1, \mathcal{A}_2\}$. The results are described in Figs. 1(a) and 1(b).

When $\phi = 0.5$, we have $\mathbb{M}_h(\{\mathcal{A}_1\}) = \mathbb{M}_k(\{\mathcal{A}_1\}) = 0.5 + 0.1i$ and $\mathbb{M}_h(\omega) = \mathbb{M}_k(\omega) = 0.5 - 0.1i$. Regardless of the variation in ω as $\{\mathcal{A}_2\}$ or $\{\mathcal{A}_1, \mathcal{A}_2\}$, the correlation coefficient measurements $\mathbb{C}(\mathbb{M}_h, \mathbb{M}_k)$ still have the largest value of 1 since $\mathbb{M}_h = \mathbb{M}_k$, which is totally correlated. Therefore, the CECC's nondegeneracy property is verified.

Conversely, from Figs. 1(a) and 1(b), it is obvious that $\mathbb{C}(\mathbb{M}_h, \mathbb{M}_k) \geq 0$ and $\mathbb{C}(\mathbb{M}_h, \mathbb{M}_k) \leq 1$, which verifies the CECC's boundedness property.

Additionally, when $\psi = 0$, $\mathbb{M}_h$ and $\mathbb{M}_k$ degrade into positive real numbers from complex numbers so that $\mathbb{M}_h(\{\mathcal{A}_1\}) = \mathbb{M}_k(\omega) = \phi$ and $\mathbb{M}_h(\omega) = \mathbb{M}_k(\{\mathcal{A}_1\}) = 1 - \phi$. In this situation, regardless of how ω changes as $\{\mathcal{A}_1\}$ or $\{\mathcal{A}_1, \mathcal{A}_2\}$, we notice that the proposed $\mathbb{C}(\mathbb{M}_h, \mathbb{M}_k)$ is exactly the same as Jiang's correlation coefficient method, as shown in Figs. 1(c) and 1(d). This result verifies that when CBBAs are degraded from complex numbers into positive real numbers, the CECC degrades into Jiang's correlation coefficient.

Specifically, when $\phi = 0$ and $\omega = \{\mathcal{A}_2\}$, we have $\mathbb{M}_h(\{\mathcal{A}_1\}) = \mathbb{M}_k(\{\mathcal{A}_2\}) = 0$ and $\mathbb{M}_h(\{\mathcal{A}_2\}) = \mathbb{M}_k(\{\mathcal{A}_1\}) = 1$; when $\phi = 1$ and $\omega = \{\mathcal{A}_2\}$, we have $\mathbb{M}_h(\{\mathcal{A}_1\}) = \mathbb{M}_k(\{\mathcal{A}_2\}) = 1$ and $\mathbb{M}_h(\{\mathcal{A}_2\}) = \mathbb{M}_k(\{\mathcal{A}_1\}) = 0$. In the above two cases, the CECC and Jiang's method obtain a result of 0. This seems reasonable because under the case where $\omega = \{\mathcal{A}_2\}$, the subsets between $\mathbb{M}_h(\{\mathcal{A}_1\})$ and $\mathbb{M}_k(\{\mathcal{A}_2\})$ or between $\mathbb{M}_k(\{\mathcal{A}_1\})$ and $\mathbb{M}_h(\{\mathcal{A}_2\})$ have no intersection. Conversely, when $\phi = 0$ and $\omega = \{\mathcal{A}_1, \mathcal{A}_2\}$, we have $\mathbb{M}_h(\{\mathcal{A}_1\}) = \mathbb{M}_k(\{\mathcal{A}_1, \mathcal{A}_2\}) = 0$ and $\mathbb{M}_h(\{\mathcal{A}_1, \mathcal{A}_2\}) = \mathbb{M}_k(\{\mathcal{A}_1\}) = 1$; and when $\phi = 1$ and $\omega = \{\mathcal{A}_1, \mathcal{A}_2\}$, we have $\mathbb{M}_h(\{\mathcal{A}_1\}) = \mathbb{M}_k(\{\mathcal{A}_1, \mathcal{A}_2\}) = 1$ and $\mathbb{M}_h(\{\mathcal{A}_1, \mathcal{A}_2\}) = \mathbb{M}_k(\{\mathcal{A}_1\}) = 0$. In these two cases, the CECC and Jiang's method obtain the result of 0.5. This also seems reasonable because in the case where $\omega = \{\mathcal{A}_1, \mathcal{A}_2\}$, the subsets between $\mathbb{M}_h(\{\mathcal{A}_1\})$ and $\mathbb{M}_k(\{\mathcal{A}_1, \mathcal{A}_2\})$ or between $\mathbb{M}_k(\{\mathcal{A}_1\})$ and $\mathbb{M}_h(\{\mathcal{A}_1, \mathcal{A}_2\})$ intersect at $\{\mathcal{A}_1\}$. Therefore, the correlation coefficient measures are equal to 0.5 instead of 0.

When ϕ changes from 0 to 0.5, regardless of whether $\omega = \{\mathcal{A}_2\}$ or $\omega = \{\mathcal{A}_1, \mathcal{A}_2\}$, $\mathbb{C}(m_1, m_2)$ is gradually increasing, as shown in Figs. 1(a), 1(b) 1(c) and 1(d). This satisfies the expected result since $\mathbb{M}_h$ and $\mathbb{M}_k$ are going to be similar when ϕ changes from 0 to 0.5. Moreover, as ϕ increases from 0.5 to 1, regardless of whether $\omega = \{\mathcal{A}_2\}$ or $\omega = \{\mathcal{A}_1, \mathcal{A}_2\}$, $\mathbb{C}(m_1, m_2)$ is gradually decreasing, which is also intuitive,

because $\mathbb{M}_h$ and $\mathbb{M}_k$ are increasingly different as ϕ changes from 0.5 to 1.

Based on Definition 5, the conflict coefficient between CBBAs is defined as follows.

Definition 6 *(Complex conflict coefficient between CBBAs) Let $\mathbb{M}_h$ and $\mathbb{M}_k$ be two CBBAs on FOD $\mathbf{\Omega}$. The complex conflict coefficient between CBBAs $\mathbb{M}_h$ and $\mathbb{M}_k$, which is denoted as $\mathbb{K}_{CBBA}(\mathbb{M}_h, \mathbb{M}_k)$, is defined by*

$$\begin{aligned}\mathbb{K}_{CBBA}(\mathbb{M}_h, \mathbb{M}_k) &= 1 - \mathbb{C}(\mathbb{M}_h, \mathbb{M}_k) \\ &= 1 - \frac{\sqrt{\langle \overrightarrow{\mathbb{M}}_h, \overrightarrow{\mathbb{M}}_k \rangle \langle \overrightarrow{\mathbb{M}}_k, \overrightarrow{\mathbb{M}}_h \rangle}}{\|\overrightarrow{\mathbb{M}}_h\| \|\overrightarrow{\mathbb{M}}_k\|}.\end{aligned} \tag{16}$$

Theorem 2 *$\mathbb{K}_{CBBA}$ has nonnegativity, symmetry, boundedness, extreme consistency, and insensitivity to refinement properties for conflict measurement [42].*

Property 3 *P 3.1 Nonnegativity: $\mathbb{K}_{CBBA}(\mathbb{M}_h, \mathbb{M}_k) \geq 0$.*

P 3.2 Symmetry: $\mathbb{K}_{CBBA}(\mathbb{M}_h, \mathbb{M}_k) = \mathbb{K}_{CBBA}(\mathbb{M}_k, \mathbb{M}_h)$.

P 3.3 Boundedness: $0 \leq \mathbb{K}_{CBBA}(\mathbb{M}_h, \mathbb{M}_k) \leq 1$.

P 3.4 Extreme consistency: 1) $\mathbb{K}_{CBBA}(\mathbb{M}_h, \mathbb{M}_k) = 0$ iff $\mathbb{M}_h$ is completely conflicting with $\mathbb{M}_k$ such that for the focal elements $\mathcal{A}_i$ and $\mathcal{A}_j$ of $\mathbb{M}_h$ and $\mathbb{M}_k$, respectively, $(\cup \mathcal{A}_i) \cap (\cup \mathcal{A}_j) = \emptyset$; 2) $\mathbb{K}_{CBBA}(\mathbb{M}_h, \mathbb{M}_k) = 1$ iff $\mathbb{M}_h$ is completely nonconflicting with $\mathbb{M}_k$.

P 3.5 Insensitivity to refinement: the complex conflict coefficient measure is insensitive to refinement so that $\mathbb{M}_h$ and $\mathbb{M}_k$ are refined from FOD $\mathbf{\Omega}$ to $\mathbf{\Omega}'$, $\mathbb{K}_{CBBA}(\mathbb{M}_1^{\mathbf{\Omega}}, \mathbb{M}_2^{\mathbf{\Omega}}) = \mathbb{K}_{CBBA}(\mathbb{M}_1^{\mathbf{\Omega}'}, \mathbb{M}_2^{\mathbf{\Omega}'})$.

Proof *(P 3.1)–(P 3.5) are trivial.*

When CBBAs $\mathbb{M}_h$ and $\mathbb{M}_k$ degrade into positive real numbers from complex numbers, we have $y = 0$ such that $\mathbb{M}(\mathcal{A}) = \mathbf{m}(\mathcal{A}) = x$. Through Eq. (15), $\mathbb{K}_{CBBA}(\overrightarrow{\mathbb{M}}_h, \overrightarrow{\mathbb{M}}_k)$ can then be represented as

$$\mathbb{K}_{CBBA}(\overrightarrow{\mathbb{M}}_h, \overrightarrow{\mathbb{M}}_k) = 1 - \frac{\langle \overrightarrow{\mathbb{M}}_h, \overrightarrow{\mathbb{M}}_k \rangle}{\|\overrightarrow{\mathbb{M}}_h\| \|\overrightarrow{\mathbb{M}}_k\|} = 1 - \frac{\langle \overrightarrow{\mathbf{m}}_h, \overrightarrow{\mathbf{m}}_k \rangle}{\|\overrightarrow{\mathbf{m}}_h\| \|\overrightarrow{\mathbf{m}}_k\|}. \tag{17}$$

According to Eq. (17), we observe that when the CBBAs are degraded from complex numbers into positive real numbers, the $\mathbb{K}_{CBBA}$ degrades into Jiang's conflict coefficient k_r [42].

Property 4 *The complex conflict coefficient $\mathbb{K}_{CBBA}$ is a generalization of Jiang's k_r [42].*

4 Comparison with Existing Methods

In this section, we provide five numerical examples to show different conflict measures' features and analyze whether they meet the properties for conflict measurement, including $|\mathbb{K}|$ [30], d_{CBBA} [43], k_r [42] and the proposed $\mathbb{K}_{CBBA}$.

Example 4 Consider two CBBAs, $\mathbb{M}_h$ and $\mathbb{M}_k$, in FOD $\mathbf{\Omega} = \{\mathcal{A}_1, \mathcal{A}_2, \mathcal{A}_3, \mathcal{A}_4\}$:

$$\begin{aligned}\mathbb{M}_h: \quad & \mathbb{M}_h(\{\mathcal{A}_1\}) = 0.5099 e^{i \arctan(0.2000)}, \\ & \mathbb{M}_h(\{\mathcal{A}_2\}) = 0.5099 e^{i \arctan(-0.2000)}, \\ & \mathbb{M}_h(\{\mathcal{A}_3\}) = 0.0, \mathbb{M}_h(\{\mathcal{A}_4\}) = 0.0; \\ \mathbb{M}_k: \quad & \mathbb{M}_k(\{\mathcal{A}_1\}) = 0.0, \mathbb{M}_k(\{\mathcal{A}_2\}) = 0.0, \\ & \mathbb{M}_k(\{\mathcal{A}_3\}) = 0.5099 e^{i \arctan(0.2000)}, \\ & \mathbb{M}_k(\{\mathcal{A}_4\}) = 0.5099 e^{i \arctan(-0.2000)}.\end{aligned}$$

In Example 4, it is obvious that for the focal elements $\mathcal{A}_i$ and $\mathcal{A}_j$ of $\mathbb{M}_h$ and $\mathbb{M}_k$, respectively, we have $(\cup \mathcal{A}_i) \cap (\cup \mathcal{A}_j) = \emptyset$. This indicates that $\mathbb{M}_h$ and $\mathbb{M}_k$ are totally conflicting, such that the conflict grade between $\mathbb{M}_h$ and $\mathbb{M}_k$ is taken to be one.

TABLE 1
Conflict measures in Example 4.

CBBAs	$\lvert\mathbb{K}\rvert$	d_{CBBA}	$\mathbb{K}_{CBBA}$
$(\mathbb{M}_h, \mathbb{M}_k)$	1	0.7211	1

By analyzing the results in Table 1, it is found that the conflict values of $|\mathbb{K}|$ and $\mathbb{K}_{CBBA}$ are 1, which is intuitive. Conversely, d_{CBBA} generates the value of 0.7211. Therefore, d_{CBBA} does not meet the extreme consistency property. Note that k_r cannot measure the conflict coefficient between CBBAs.

Example 5 Consider two CBBAs, $\mathbb{M}_h$ and $\mathbb{M}_k$, in FOD $\mathbf{\Omega} = \{\mathcal{A}_1, \mathcal{A}_2, \mathcal{A}_3, \mathcal{A}_4\}$:

$$\begin{aligned}\mathbb{M}_h: \quad & \mathbb{M}_h(\{\mathcal{A}_1\}) = 0.2693 e^{i \arctan(0.4000)}, \\ & \mathbb{M}_h(\{\mathcal{A}_2\}) = 0.2693 e^{i \arctan(0.4000)}, \\ & \mathbb{M}_h(\{\mathcal{A}_3\}) = 0.2693 e^{i \arctan(-0.4000)}, \\ & \mathbb{M}_h(\{\mathcal{A}_4\}) = 0.2693 e^{i \arctan(-0.4000)}; \\ \mathbb{M}_k: \quad & \mathbb{M}_k(\{\mathcal{A}_1\}) = 0.2693 e^{i \arctan(0.4000)}, \\ & \mathbb{M}_k(\{\mathcal{A}_2\}) = 0.2693 e^{i \arctan(0.4000)}, \\ & \mathbb{M}_k(\{\mathcal{A}_3\}) = 0.2693 e^{i \arctan(-0.4000)}, \\ & \mathbb{M}_k(\{\mathcal{A}_4\}) = 0.2693 e^{i \arctan(-0.4000)}.\end{aligned}$$

In Example 5, obviously, $\mathbb{M}_h$ is the same as $\mathbb{M}_k$. This means that $\mathbb{M}_h$ and $\mathbb{M}_k$ are totally nonconflicting, where the conflict between $\mathbb{M}_h$ and $\mathbb{M}_k$ is taken to be 0.

TABLE 2
Conflict measures in Example 5.

CBBAs	$\lvert\mathbb{K}\rvert$	d_{CBBA}	$\mathbb{K}_{CBBA}$
$(\mathbb{M}_h, \mathbb{M}_k)$	0.7900	0	0

By analyzing the results in Table 2, it can be seen that the conflict degrees calculated by d_{CBBA} and $\mathbb{K}_{CBBA}$ are zero, which achieves the expected result, whereas $|\mathbb{K}| = 0.79$ and does not meet the extreme consistency property.

Example 6 Consider two CBBAs, $\mathbb{M}_h$ and $\mathbb{M}_k$, in $\mathbf{\Omega} =$

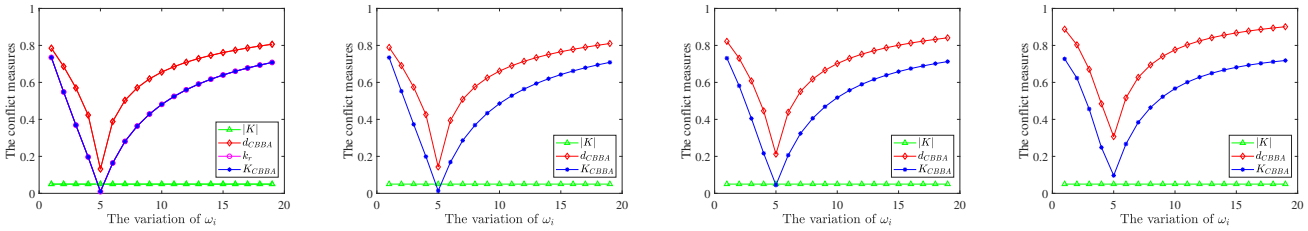

(a) $\phi = 0$. (b) $\phi = 0.1$. (c) $\phi = 0.3$. (d) $\phi = 0.5$.

Fig. 2. Comparisons of conflict coefficient measures in Example 7.

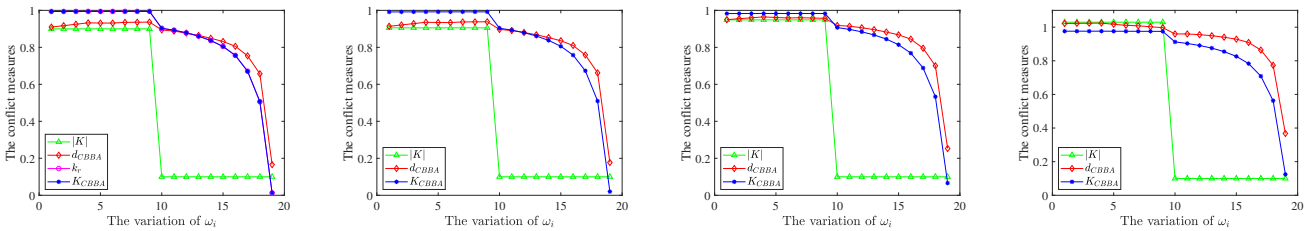

(a) $\psi = 0$. (b) $\psi = 0.1$. (c) $\psi = 0.3$. (d) $\psi = 0.5$.

Fig. 3. Comparisons of the conflict coefficient measures in Example 8.

$\{\mathcal{A}_1, \mathcal{A}_2\}$ and $\mathbf{\Omega}' = \{\mathcal{A}_1, \mathcal{A}_2, \mathcal{A}_3\}$, respectively:

$$\begin{aligned} \mathbb{M}_h: \quad & \mathbb{M}_h(\{\mathcal{A}_1\}) = 0.8139e^{i\arctan(0.1875)}, \\ & \mathbb{M}_h(\{\mathcal{A}_2\}) = 0.2500e^{i\arctan(-0.7500)}; \\ \mathbb{M}_k: \quad & \mathbb{M}_k(\{\mathcal{A}_1\}) = 0.2500e^{i\arctan(-0.7500)}, \\ & \mathbb{M}_k(\{\mathcal{A}_2\}) = 0.8139e^{i\arctan(0.1875)}. \end{aligned}$$

In Example 6, consider the same CBBAs $\mathbb{M}_h$ and $\mathbb{M}_k$ in different FODs $\mathbf{\Omega} = \{\mathcal{A}_1, \mathcal{A}_2\}$ and $\mathbf{\Omega}' = \{\mathcal{A}_1, \mathcal{A}_2, \mathcal{A}_3\}$, respectively. As expected, the conflicts between $\mathbb{M}_h$ and $\mathbb{M}_k$ in FODs $\mathbf{\Omega}$ and $\mathbf{\Omega}'$ are taken to be equal.

TABLE 3
Conflict measures in Example 6.

CBBAs	$\lvert\mathbb{K}\rvert$	d_{CBBA}	$\mathbb{K}_{CBBA}$
$(\mathbb{M}_h, \mathbb{M}_k)^{\mathbf{\Omega}}$	0.6600	0.6708	0.6207
$(\mathbb{M}_h, \mathbb{M}_k)^{\mathbf{\Omega}'}$	0.6600	0.6708	0.6207

As shown in Table 3, we note that $|\mathbb{K}| = 0.66$, $d_{CBBA} = 0.6708$, and $\mathbb{K}_{CBBA} = 0.6207$, regardless of whether in $\mathbf{\Omega}$ or $\mathbf{\Omega}'$. These results meet our expectations, where $|\mathbb{K}|$, d_{CBBA} and $\mathbb{K}_{CBBA}$ satisfy the insensitivity to refinement property.

Accordingly, the three examples show the disadvantages of well-known related works. The proposed $\mathbb{K}_{CBBA}$ satisfies the properties for conflict measurement, whereas $|\mathbb{K}|$ and d_{CBBA} do not meet the extreme consistency property. Next, we discuss two examples to show the effectiveness of $\mathbb{K}_{CBBA}$.

Example 7 Consider two CBBAs, $\mathbb{M}_h$ and $\mathbb{M}_k$, in FOD $\mathbf{\Omega} = \{\mathcal{A}_1, \mathcal{A}_2, \ldots, \mathcal{A}_{19}\}$:

$$\begin{aligned} \mathbb{M}_h: \quad & \mathbb{M}_h(\mathbf{\Omega}) = 0.1, \mathbb{M}_h(\{\mathcal{A}_2, \mathcal{A}_3, \mathcal{A}_4\}) = 0.05 + \phi i, \\ & \mathbb{M}_h(\{\mathcal{A}_7\}) = 0.05, \mathbb{M}_h(\omega_i) = 0.8 - \phi i; \\ \mathbb{M}_k: \quad & \mathbb{M}_k(\{\mathcal{A}_1, \mathcal{A}_2, \mathcal{A}_3, \mathcal{A}_4, \mathcal{A}_5\}) = 1. \end{aligned}$$

TABLE 4
The variation in ω_i.

i	ω_i
1	$\{\mathcal{A}_1\}$
2	$\{\mathcal{A}_1, \mathcal{A}_2\}$
3	$\{\mathcal{A}_1, \mathcal{A}_2, \mathcal{A}_3\}$
4	$\{\mathcal{A}_1, \mathcal{A}_2, \mathcal{A}_3, \mathcal{A}_4\}$
5	$\{\mathcal{A}_1, \mathcal{A}_2, \mathcal{A}_3, \mathcal{A}_4, \mathcal{A}_5\}$
6	$\{\mathcal{A}_1, \mathcal{A}_2, \mathcal{A}_3, \mathcal{A}_4, \mathcal{A}_5, \mathcal{A}_6\}$
7	$\{\mathcal{A}_1, \mathcal{A}_2, \mathcal{A}_3, \mathcal{A}_4, \mathcal{A}_5, \mathcal{A}_6, \mathcal{A}_7\}$
8	$\ldots$
19	$\{\mathcal{A}_1, \mathcal{A}_2, \mathcal{A}_3, \mathcal{A}_4, \mathcal{A}_5, \ldots, \mathcal{A}_{19}\}$

In Example 7, the ω_i of $\mathbb{M}_h$ varies from $\{\mathcal{A}_1\}$ to $\{\mathcal{A}_1, \ldots, \mathcal{A}_{19}\}$ in Table 4. Here, $\mathbb{M}_k$ has one focal element: $\mathbb{M}_k(\{\mathcal{A}_1, \mathcal{A}_2, \mathcal{A}_3, \mathcal{A}_4, \mathcal{A}_5\}) = 1$. The expected result in this example should be that when the subset ω_i of $\mathbb{M}_h$ becomes $\{\mathcal{A}_1, \mathcal{A}_2, \mathcal{A}_3, \mathcal{A}_4, \mathcal{A}_5\}$, the conflict degree between CBBAs $\mathbb{M}_h$ and $\mathbb{M}_k$ is taken to be the minimal value.

When $\phi = 0$, which means that the CBBAs are degraded from complex numbers into positive real numbers, $\mathbb{K}_{CBBA}$ degrades into Jiang's conflict coefficient k_r. Therefore, in this situation, $\mathbb{K}_{CBBA}$ has the same conflict measure as Jiang's k_r, as shown in Fig. 2(a). When ϕ varies from 0.1 to 0.3 and 0.5, k_r cannot measure the conflict coefficient between CBBAs. d_{CBBA} and the proposed $\mathbb{K}_{CBBA}$ can well measure the conflict degree between CBBAs, while $|\mathbb{K}|$ always maintains a value of 0.05, which cannot distinguish the conflict, regardless of how the ω_i changes and ϕ varies, as shown in Figs. 2(a), 2(b), 2(c) and 2(d).

From the result in Fig. 2, when the ω_i of $\mathbb{M}_h$ varies from $\{\mathcal{A}_1\}$ to $\{\mathcal{A}_1, \mathcal{A}_2, \mathcal{A}_3, \mathcal{A}_4, \mathcal{A}_5\}$, d_{CBBA} and $\mathbb{K}_{CBBA}$ become increasingly smaller. In particular, when $i = 5$,

$\mathbb{M}_h$ has the subset $\{\mathcal{A}_1, \mathcal{A}_2, \mathcal{A}_3, \mathcal{A}_4, \mathcal{A}_5\}$. d_{CBBA} achieves its minimum values of 0.1315, 0.1427, 0.2119 and 0.3070 when ϕ is equal to 0, 0.1, 0.3 and 0.5, respectively. $\mathbb{K}_{CBBA}$ achieves its minimum values of 0.0094, 0.0257, 0.0688 and 0.1259 when ϕ is equal to 0, 0.1, 0.3 and 0.5, respectively. As ω_i increases from $\{\mathcal{A}_1, \mathcal{A}_2, \mathcal{A}_3, \mathcal{A}_4, \mathcal{A}_5\}$ to $\{\mathcal{A}_1, \ldots, \mathcal{A}_{19}\}$, the conflict degrees generated by d_{CBBA} and $\mathbb{K}_{CBBA}$ increase, which achieves the expected result.

TABLE 5
The variation in ξ_i.

i	ξ_i
1-10	ω_i
11	$\{\mathcal{A}_2, \mathcal{A}_3, \mathcal{A}_4, \mathcal{A}_5, \mathcal{A}_6, \mathcal{A}_7, \mathcal{A}_8, \mathcal{A}_9, \mathcal{A}_{10}\}$
12	$\{\mathcal{A}_3, \mathcal{A}_4, \mathcal{A}_5, \mathcal{A}_6, \mathcal{A}_7, \mathcal{A}_8, \mathcal{A}_9, \mathcal{A}_{10}\}$
13	$\{\mathcal{A}_4, \mathcal{A}_5, \mathcal{A}_6, \mathcal{A}_7, \mathcal{A}_8, \mathcal{A}_9, \mathcal{A}_{10}\}$
14	$\{\mathcal{A}_5, \mathcal{A}_6, \mathcal{A}_7, \mathcal{A}_8, \mathcal{A}_9, \mathcal{A}_{10}\}$
15	$\{\mathcal{A}_6, \mathcal{A}_7, \mathcal{A}_8, \mathcal{A}_9, \mathcal{A}_{10}\}$
16	$\{\mathcal{A}_7, \mathcal{A}_8, \mathcal{A}_9, \mathcal{A}_{10}\}$
17	$\{\mathcal{A}_8, \mathcal{A}_9, \mathcal{A}_{10}\}$
18	$\{\mathcal{A}_9, \mathcal{A}_{10}\}$
19	$\{\mathcal{A}_{10}\}$

Example 8 Consider two CBBAs, $\mathbb{M}_h$ and $\mathbb{M}_k$, in FOD $\mathbf{\Omega} = \{\mathcal{A}_1, \mathcal{A}_2, \ldots, \mathcal{A}_{19}\}$:

$$\begin{aligned} \mathbb{M}_h: \quad & \mathbb{M}_h(\mathbf{\Omega}) = 0.1 - \psi i, \mathbb{M}_h(\{\mathcal{A}_2, \mathcal{A}_3, \mathcal{A}_4\}) = 0.05, \\ & \mathbb{M}_h(\{\mathcal{A}_7\}) = 0.05, \mathbb{M}_h(\xi_i) = 0.8 + \psi i; \\ \mathbb{M}_k: \quad & \mathbb{M}_k(\{\mathcal{A}_{10}\}) = 1. \end{aligned}$$

In Example 8, the subset ξ_i of $\mathbb{M}_h$ changes from ξ_1 to ξ_{19} in Table 5. As $i = 1, 2, \ldots, 10$, ξ_i is equal to ω_i. When i changes from 11 to 19, the ξ_i of $\mathbb{M}_h$ is trimmed from its first element until it becomes $\{\mathcal{A}_{10}\}$. Here, $\mathbb{M}_k$ has one focal element: $\mathbb{M}_k(\{\mathcal{A}_{10}\}) = 1$. The expected result in this example should be that when subset ξ_i of $\mathbb{M}_h$ becomes $\{\mathcal{A}_{10}\}$, the conflict degree between CBBAs $\mathbb{M}_h$ and $\mathbb{M}_k$ should be the minimal value.

When $\psi = 0$, which indicates that the CBBAs are degraded from complex numbers into positive real numbers, $\mathbb{K}_{CBBA}$ degrades into Jiang's conflict coefficient k_r, where $\mathbb{K}_{CBBA}$ has the same conflict measure as k_r, as shown in Fig. 3(a). When ϕ varies from 0.1 to 0.3 and 0.5, k_r cannot measure the conflict coefficient between CBBAs. From Figs. 3(a), 3(b), 3(c) and 3(d), d_{CBBA} and the proposed $\mathbb{K}_{CBBA}$ are preferred to measure the conflict between CBBAs rather than $|\mathbb{K}|$ since $|\mathbb{K}|$ always maintains a certain value as i changes from 1 to 9 and from 10 to 19.

When i increases to 10, since $\mathbb{M}_h$ includes $\{\mathcal{A}_{10}\}$, the conflict measures are taken to be smaller than those of other cases $i = 1, \ldots, 9$. From Fig. 3, we can see that d_{CBBA} and $\mathbb{K}_{CBBA}$ satisfy the expected result. As ξ_i changes from 11 to 19, because $\{\mathcal{A}_2, \ldots, \mathcal{A}_{10}\}$ gradually decreases to $\{\mathcal{A}_{10}\}$, the d_{CBBA} and $\mathbb{K}_{CBBA}$ methods have increasingly smaller conflict degrees. In particular, when $i = 19$, d_{CBBA} achieves its minimum values of 0.1658, 0.1772, 0.2531 and 0.3678 when ψ is equal to 0, 0.1, 0.3 and 0.5, respectively; $\mathbb{K}_{CBBA}$ achieves its minimum values of 0.0128, 0.0391, 0.0957 and 0.1508 when ψ is equal to 0, 0.1, 0.3 and 0.5, respectively.

TABLE 6
Characteristics of different conflict measures.

Situations	Conflict measures			
	$\lvert\mathbb{K}\rvert$ [30]	d_{CBBA} [43]	k_r [42]	$\mathbb{K}_{CBBA}$
Real number	✓	✓	✓	✓
Complex number	✓	✓	✗	✓
Nonnegativity	✓	✓	✓	✓
Symmetry	✓	✓	✓	✓
Extreme consistency	✗	✗	✓	✓
Insensitivity to refinement	✓	✓	✓	✓

Accordimgly, from Examples 7 and 8, it is obvious that the proposed $\mathbb{K}_{CBBA}$ and d_{CBBA} are more effective at distinguishing conflict. Recall Example 4; since d_{CBBA} does not meet the extreme consistency property, the proposed $\mathbb{K}_{CBBA}$ is superior to the related works, as it is more effective in measuring the conflict between CBBAs.

In summary, the characteristics of different conflict measures are summarized in Table 6.

5 CECC-BASED WEIGHTED DISCOUNTING MULTISOURCE INFORMATION FUSION ALGORITHM

Multisource information fusion problems have attracted much attention [51–53]. It is considered that CECC can well measure conflicts between CBBAs. To overcome the limitation of CET-based expert systems when facing highly conflicting CBBAs, we take advantage of CECC to obtain the weights to discount the original CBBAs. In this way, the impacts of highly conflicting CBBAs on the system can be alleviated to better support decision-making. Therefore, in this section, a weighted discounting multisource information fusion algorithm called the CECC-WDMSIF is designed based on the CECC to improve the performance of CET-based expert systems.

Problem statement: Let $\{C_1, ..., C_p, ..., C_n\}$ be a set of objectives in FOD $\mathbf{\Omega}$. Let $\mathcal{M} = \{\mathbb{M}_1, ..., \mathbb{M}_q, ..., \mathbb{M}_s\}$ be a set of CBBAs modeled based on the collected data from multiple sources. Then, according to the given CBBAs, a decision can be made after implementing the CECC-based WDMSIF algorithm.

Step 1: On the basis of the CECC, a correlation matrix is constructed between arbitrary CBBAs:

$$\mathrm{M}_{\mathbb{C}} = \begin{bmatrix} \mathbb{C}(\mathbb{M}_1, \mathbb{M}_1) & \cdots & \mathbb{C}(\mathbb{M}_1, \mathbb{M}_s) \\ \vdots & \vdots & \vdots \\ \mathbb{C}(\mathbb{M}_s, \mathbb{M}_1) & \cdots & \mathbb{C}(\mathbb{M}_s, \mathbb{M}_s) \end{bmatrix}. \tag{18}$$

Step 2: The support degree for $\mathbb{M}_q$ is calculated:

$$\mathrm{Sud}(\mathbb{M}_q) = \sum_{h=1|h\neq q}^{s} \mathbb{C}(\mathbb{M}_q, \mathbb{M}_h). \tag{19}$$

Step 3: A weight in terms of $\mathbb{M}_q$ is calculated:

$$\lambda_q = \frac{\mathrm{Sud}(\mathbb{M}_q)}{\max\limits_{1\leq q\leq s} \mathrm{Sud}(\mathbb{M}_q)}. \tag{20}$$

Step 4: In accordance with λ, the discounting evidence $\widetilde{\mathbb{M}}$ is obtained:

$$\mathbb{M}_q^{\lambda} = \begin{cases} \lambda_q \mathbb{M}_q(\mathcal{A}_j), & \text{if } \mathcal{A}_j \subset \mathbf{\Omega}, \\ 1 - \lambda_q + \lambda_q \mathbb{M}_q(\mathcal{A}_j), & \text{if } \mathcal{A}_j = \mathbf{\Omega}, \mathcal{A}_j \neq \emptyset. \end{cases} \tag{21}$$

Step 5: $\mathbb{M}_q^{\lambda}$ are fused by DCR:

$$\dot{\mathbb{M}}^{\lambda} = (((\mathbb{M}_1^{\lambda} \oplus \mathbb{M}_2^{\lambda}) \oplus \cdots \oplus \mathbb{M}_q^{\lambda}) \oplus \cdots \oplus \mathbb{M}_s^{\lambda}). \tag{22}$$

Step 6: By using the complex Pignistic belief transformation (CPBT) function [28], the belief values of singletons in terms of these objectives are calculated:

$$\mathrm{CBet}(C_p) = \sum_{C_p \in \mathcal{A}_j} \frac{\dot{\mathbb{M}}^{\lambda}(\mathcal{A}_j)}{|\mathcal{A}_j|}, \tag{23}$$

where $|\mathcal{A}_j|$ represents the cardinality of $\mathcal{A}_j$.

Step 7: The φ with the largest $|\mathrm{CBet}(C_\varphi)|$ is recorded:

$$\varphi = \arg\max_{1 \leq p \leq n} \{|\mathrm{CBet}(C_p)|\}. \tag{24}$$

Step 8: Hypothesis C_φ is selected as the predicted target for decision making.

This CECC-based weighted discounting multisource information fusion algorithm for CET-based expert systems is given in Algorithm 1.

Algorithm 1: CECC-based weighted discounting multisource information fusion for CET-based expert systems.

Input: $\mathbf{\Omega} = \{C_1, ..., C_p, ..., C_n\}$; $\mathcal{M} = \{\mathbb{M}_1, ..., \mathbb{M}_q, ..., \mathbb{M}_s\}$;
Output: Decision making;
for $q = 1; q \leq s$ **do**
  Construct a matrix of correlation $\mathrm{M_C}$ with Eq. (18);
end
for $q = 1; q \leq s$ **do**
  Calculate the support degree of $\mathrm{Sud}(\mathbb{M}_q)$ with Eq. (19);
end
for $q = 1; q \leq s$ **do**
  Produce the weight of λ_q with Eq. (20);
end
for $q = 1; q \leq s$ **do**
  Calculate the discounting evidence of $\mathbb{M}_q^{\lambda}$ with Eq. (21);
end
for $q = 1; q \leq s$ **do**
  Obtain the fused $\dot{\mathbb{M}}^{\lambda}$ with Eq. (22);
end
for $q = 1; q \leq s$ **do**
  Obtain the belief values of singletons in terms of these objectives with Eq. (23);
end
Select $\varphi = \arg\max_{1 \leq p \leq n} \{|\mathrm{CBet}(C_p)|\}$ with Eq. (24);
Hypothesis C_p is selected as the predicted target for decision making.

6 Application to Pattern Classification

Pattern classification has attracted much attention in recent decades [54, 55]. In this section, we apply the CECC-WDMSIF algorithm to pattern classification to validate its practicability. Furthermore, we compare the proposed CECC-WDMSIF algorithm to well-known related works on several real-world datasets from the UC Irvine (UCI) Machine Learning Repository (http://archive.ics.uci.edu/ml/) to validate its practicability and superiority.

TABLE 7
Summarized information of the experimental datasets in Section 6.1.

Dataset	#Sample	#Class	#Attribute	Missing Value
Iris	150	3	4	NO
Wine	178	3	13	NO
Heart	270	2	13	NO
Parkinson's	197	2	22	NO
Australian	690	2	14	YES

6.1 Implementation and evaluation of the CECC-WDMSIF

Here, the proposed CECC-WDMSIF has been successfully verified on the five datasets of Iris, Wine, Heart, Parkinson's and Australian, where the information of sample, class, attribute and missing value are summarized in Table 7.

For each dataset, multiple attributes can be considered as independent sources to supply different information. In particular, when a dataset has a few missing values or involves noise, it is desirable that a reliable decision be made according to such multisource information. The first primary merit of the CECC-WDMSIF is that the missing values of datasets can be considered as having a status of "ignorance" for the actual state in the evidence theory framework. This indicates that we have no idea about which class the missing value belongs to in the situation of "ignorance", so the complex mass function can be constructed as $\mathbb{M}(\Omega) = 1$. Therefore, it is not necessary to manage the missing values of datasets externally. The second primary merit of the CECC-WDMSIF is that the influence caused by dataset noise on the fusion system can be alleviated by applying the weighted discounting process for complex evidence. The decision level can be improved by fusing multi-attribute information through the CECC-WDMSIF.

To implement the proposed CECC-WDMSIF, CBBAs should first be generated from the multiattributes of each dataset. By integrating the extended method of [56] with the $e^{i\theta}$ function, the corresponding CBBAs are acquired based on the training samples. Of note, we also provide an example to illustrate CBBA generation in accordance with different attributes of a testing sample in terms of Iris dataset in Appendix. Furthermore, for each testing sample, the CECC-WDMSIF is implemented to fuse the generated CBBAs from the multi-attributes to classify the testing sample within a certain pattern for decision-making support. Through analyzing the computational complexities of the CECR-MSIF and the proposed CECC-WDMSIF algorithms, it is noticed that in the case of s CBBAs and n classes, both of them have the same computational complexity of $O(s2^n)$.

Since the variation of θ impacts CBBA generation, to study the performance of the proposed CECC-WDMSIF in this situation, all data are selected as training data and testing data in this experiment. After executing the CECC-WDMSIF, we evaluate its classification accuracy and standard deviation regarding θ variation in the range of $[0, 2\pi]$. In particular, when $\theta = 0$, the CBBAs convert to traditional BBAs. Meanwhile, the proposed CECC-WDMSIF requires to be compared with the classic CECR-MSIF [30], because both of them can provide uncertainty reasoning for not only real-

TABLE 8
Comparison of the classification accuracy and standard deviation in a five-fold cross validation with θ variation in Section 6.1.

Times	Accuracy	Iris		Wine		Heart		Parkinson's		Australian		Avg	
		CECR-MSIF	CECC-WDMSIF	CECR-MSIF	CECC-WDMSIF	CECR-MSIF	CECC-WDMSIF	CECR-MSIF	CECC-WDMSIF	CECR-MSIF	CECC-WDMSIF	CECR-MSIF	CECC-WDMSIF
1st	Max	96.67%	96.67%	94.12%	94.12%	79.63%	83.33%	89.47%	94.74%	90.51%	89.05%	90.08%	91.58%
	Min	86.67%	86.67%	73.53%	79.41%	61.11%	75.93%	60.53%	76.32%	86.86%	83.94%	73.74%	80.45%
	Avg	88.95%	91.31%	85.18%	88.75%	77.16%	80.86%	79.98%	84.31%	89.61%	86.35%	84.18%	86.32%
	Std	2.76%	3.10%	4.51%	3.58%	3.33%	2.40%	6.03%	4.89%	0.85%	1.30%	3.50%	3.05%
2nd	Max	96.67%	96.67%	94.12%	94.12%	85.19%	83.33%	86.84%	84.21%	83.21%	86.86%	89.20%	89.04%
	Min	86.67%	86.67%	70.59%	82.35%	68.52%	74.07%	52.63%	52.63%	54.74%	81.75%	66.63%	75.50%
	Avg	91.18%	92.22%	88.64%	89.39%	78.00%	80.14%	76.83%	76.21%	78.82%	84.43%	82.69%	84.48%
	Std	2.63%	3.07%	5.59%	3.50%	5.50%	2.94%	7.07%	5.83%	6.17%	1.24%	5.39%	3.31%
3th	Max	96.67%	96.67%	97.06%	97.06%	88.89%	88.89%	86.84%	86.84%	91.24%	87.59%	92.14%	91.41%
	Min	80.00%	83.33%	67.65%	85.29%	55.56%	79.63%	44.74%	52.63%	75.91%	83.94%	64.77%	76.97%
	Avg	90.52%	91.31%	90.37%	91.52%	80.94%	84.93%	75.75%	78.64%	87.72%	85.73%	85.06%	86.43%
	Std	5.17%	3.85%	6.46%	3.67%	6.29%	2.23%	8.83%	7.12%	3.40%	0.73%	6.03%	3.52%
4th	Max	93.33%	93.33%	91.18%	94.12%	90.74%	87.04%	81.58%	86.84%	84.67%	86.86%	88.30%	89.64%
	Min	83.33%	90.00%	67.65%	76.47%	51.85%	72.22%	50.00%	71.05%	76.64%	81.02%	65.89%	78.15%
	Avg	91.50%	92.55%	84.26%	87.43%	80.07%	81.66%	76.16%	78.02%	81.41%	82.77%	82.68%	84.49%
	Std	3.12%	1.41%	6.35%	5.94%	7.29%	4.04%	7.21%	3.33%	1.88%	1.38%	5.17%	3.22%
5th	Max	100.0%	100.0%	100.0%	97.30%	87.04%	88.89%	87.50%	80.00%	89.21%	85.61%	92.75%	90.36%
	Min	93.33%	93.33%	83.78%	89.19%	70.37%	79.63%	50.00%	52.50%	81.29%	79.14%	75.76%	78.76%
	Avg	95.56%	97.45%	91.79%	91.63%	84.10%	86.93%	74.66%	72.30%	84.72%	82.51%	86.16%	86.16%
	Std	3.07%	1.93%	3.86%	2.69%	3.18%	2.18%	9.01%	7.24%	2.39%	1.19%	4.30%	3.05%
1st∼5th (Average)	Max	96.67%	96.67%	95.29%	95.34%	86.30%	86.30%	86.45%	86.53%	87.77%	87.20%	90.49%	90.41%
	Min	86.00%	88.00%	72.64%	82.54%	61.48%	76.30%	51.58%	61.03%	75.09%	81.96%	69.36%	77.97%
	Avg	91.54%	92.97%	88.05%	89.74%	80.05%	82.90%	76.68%	77.90%	84.46%	84.36%	84.15%	**85.57%**
	Std	3.35%	2.68%	5.35%	3.87%	5.12%	2.76%	7.63%	5.68%	2.94%	1.17%	4.88%	**3.23%**

TABLE 9
Comparison of the different average accuracy and standard deviations from the maximal accuracy and minimal standard deviation in terms of different datasets for a five-fold cross evaluation in Section 6.1.

1st∼5th (Average)	Iris		Wine		Heart		Parkinson's		Australian		ACC	
	CECR-MSIF	CECC-WDMSIF	CECR-MSIF	CECC-WDMSIF	CECR-MSIF	CECC-WDMSIF	CECR-MSIF	CECC-WDMSIF	CECR-MSIF	CECC-WDMSIF	CECR-MSIF	CECC-WDMSIF
Max	0.00%	0.00%	0.05%	0.00%	0.00%	0.00%	0.08%	0.00%	0.00%	0.57%	0.13%	0.57%
Min	2.00%	0.00%	9.90%	0.00%	14.81%	0.00%	9.45%	0.00%	6.87%	0.00%	43.03%	0.00%
Avg	1.42%	0.00%	1.70%	0.00%	2.85%	0.00%	1.22%	0.00%	0.00%	0.10%	7.20%	0.10%
Std	0.67%	0.00%	1.48%	0.00%	2.36%	0.00%	1.95%	0.00%	1.77%	0.00%	8.24%	0.00%
ACC	4.10%	**0.00%**	13.13%	**0.00%**	20.03%	**0.00%**	12.70%	**0.00%**	8.64%	**0.67%**	58.60%	**0.67%**

TABLE 10
Comparison of the classification accuracy and standard deviations generated by different methods in Section 6.2.

Dataset	Classifiers								Evidence theory-based MSIF			
	NaB	NMC	kNN	REPTree	SVM	SVM-RBF	MlP	RBFN	kNN-DST	NDC	EvC	CECC-WDMSIF
Iris	94.67%	90.67%	95.33%	92.00%	94.67%	94.67%	93.33%	92.67%	95.33%	94.00%	94.67%	**96.67%**
Wine	95.51%	70.44%	70.19%	84.92%	96.62%	96.63%	94.93%	95.49%	93.84%	96.63%	**97.17%**	95.34%
Heart	82.59%	60.37%	57.78%	70.74%	83.70%	82.96%	75.19%	81.85%	76.30%	82.59%	83.70%	**86.30%**
Parkinson's	68.75%	70.77%	83.02%	80.94%	70.13%	81.03%	74.39%	82.05%	78.01%	70.26%	81.64%	**86.53%**
Australian	79.56%	64.21%	67.40%	80.59%	80.29%	79.86%	82.32%	82.61%	78.41%	80.01%	80.60%	**87.20%**
Avg	84.22%	71.29%	74.74%	81.84%	85.08%	87.03%	84.03%	86.93%	84.38%	84.70%	87.56%	**90.41%**
Std	10.00%	10.45%	13.07%	6.90%	9.73%	7.13%	8.71%	5.91%	8.38%	9.63%	6.95%	**4.60%**

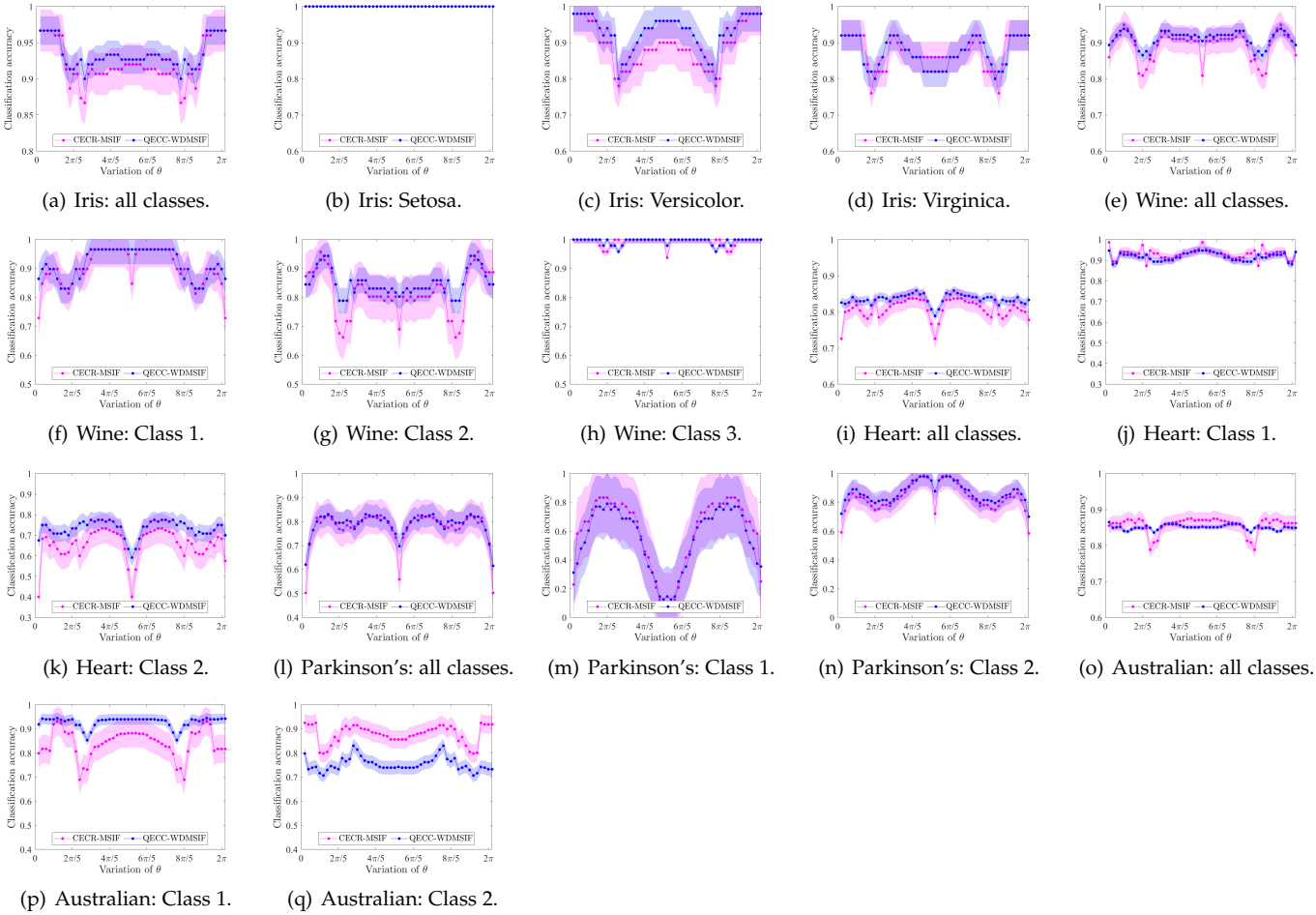

(a) Iris: all classes. (b) Iris: Setosa. (c) Iris: Versicolor. (d) Iris: Virginica. (e) Wine: all classes.

(f) Wine: Class 1. (g) Wine: Class 2. (h) Wine: Class 3. (i) Heart: all classes. (j) Heart: Class 1.

(k) Heart: Class 2. (l) Parkinson's: all classes. (m) Parkinson's: Class 1. (n) Parkinson's: Class 2. (o) Australian: all classes.

(p) Australian: Class 1. (q) Australian: Class 2.

Fig. 4. The performance of the CECR-MSIF and CECC-WDMSIF as a variation of θ in Section 6.1 (the broken line represents the classification accuracy, and the shadow represents the standard deviation).

number-modeled information but also complex-number-modeled information. The results of these two methods are depicted in Fig. 4. Specifically, Fig. 4(a) presents their classification accuracies for all classes of the Iris dataset, while Fig. 4(b), Fig. 4(c) and Fig. 4(d) present their classification accuracies for each class. Fig. 4(e) presents their classification accuracies for all classes of the Wine dataset, while Fig. 4(f), Fig. 4(g) and Fig. 4(h) present their classification accuracies for each class. Fig. 4(i) presents their classification accuracies for all classes of the Heart dataset, while Fig. 4(j) and Fig. 4(k) present their classification accuracies for each class. Fig. 4(l) presents their classification accuracies of all classes of the Parkinson's dataset, while Fig. 4(m) and Fig. 4(n) present their classification accuracies for each class. Fig. 4(o) presents their classification accuracies for all classes of the Australian dataset, while Fig. 4(p) and Fig. 4(q) present their classification accuracies for each class. Correspondingly, according to the variation of θ, Table 12A shows their maximum (Max), minimum (Min), and average (Avg) accuracies for each class, all classes, and the standard deviation (Std) of accuracy.

To compare the relative performance of the proposed CECC-WDMSIF with that of the CECR-MSIF, we use the metrics including Max, Min, Avg, and Std of accuracy of all classes. According to the results of each dataset in Table 12A, the different accuracies from the maximal accuracy and the different standard deviations from the minimal standard deviation for each dataset are calculated in Table 13A. Next, these differences are accumulated over five UCI datasets (which is denoted as ACC in Table 13A) to evaluate the relative performance of each fusion method. In Table 13A, the best performance is highlighted in bold style. The proposed CECC-WDMSIF achieves the best performance in four of five cases and is only inferior to the CECR-MSIF for the Australian dataset. Moreover, for the proposed CECC-WDMSIF, the total accumulated difference across the five UCI datasets and in the Max, Min, Avg and Std of accuracy of all classes is only 2.86%, whereas for the CECR-MSIF, its total accumulated difference is 49.12%. Therefore, the total difference from the best performing CECR-MSIF is approximately 17.19 times greater than that of the proposed CECC-WDMSIF.

A five-fold cross validation is carried out, where four folds (80%) of the total data are randomly chosen as training data, while the leftover one fold (20%) of the total data, serves as testing data. We repeat this procedure five times and then average the Max, Min, Avg and Std of accuracy of all classes for each of the five runs for further comparison. Of note, the results about performance of CECR-MSIF and CECC-WDMSIF are shown in Table 8. For all but

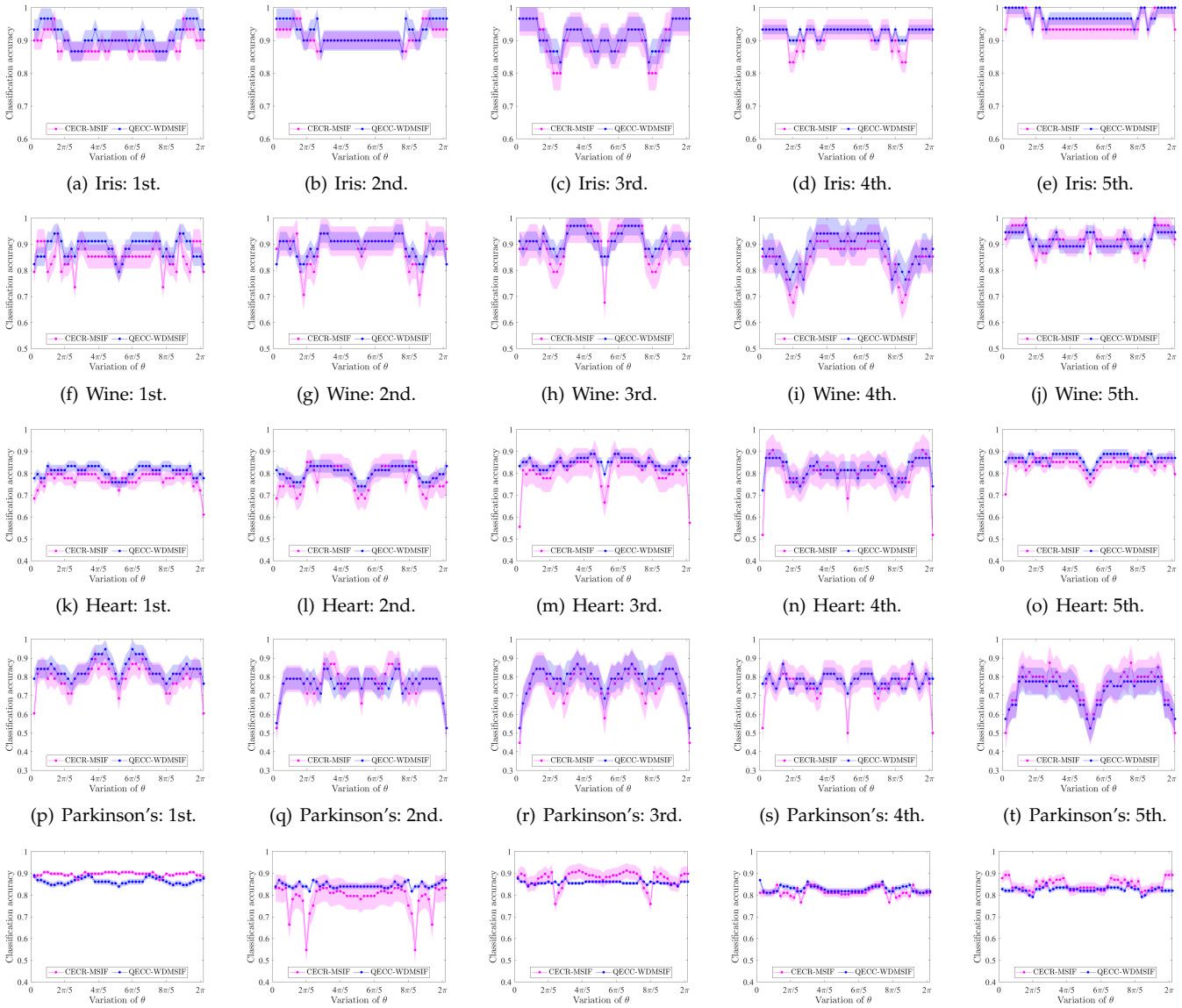

(a) Iris: 1st. (b) Iris: 2nd. (c) Iris: 3rd. (d) Iris: 4th. (e) Iris: 5th.

(f) Wine: 1st. (g) Wine: 2nd. (h) Wine: 3rd. (i) Wine: 4th. (j) Wine: 5th.

(k) Heart: 1st. (l) Heart: 2nd. (m) Heart: 3rd. (n) Heart: 4th. (o) Heart: 5th.

(p) Parkinson's: 1st. (q) Parkinson's: 2nd. (r) Parkinson's: 3rd. (s) Parkinson's: 4th. (t) Parkinson's: 5th.

(u) Australian: 1st. (v) Australian: 2nd. (w) Australian: 3rd. (x) Australian: 4th. (y) Australian: 5th.

Fig. 5. The performance of the CECR-MSIF and CECC-WDMSIF in a five-fold cross validation in Section 6.1 (the broken line represents the classification accuracy, and the shadow represents the standard deviation).

TABLE 11
Comparison of the difference between the accuracy and standard deviation and the maximal accuracy and minimal standard deviations for eleven different methods under several datasets in Section 6.2.

Dataset	Classifiers								Evidence theory-based MSIF			
	NaB	NMC	kNN	REPTree	SVM	SVM-RBF	MlP	RBFN	kNN-DST	NDC	EvC	CECC-WDMSIF
Iris	2.00%	6.00%	1.34%	4.67%	2.00%	2.00%	3.34%	4.00%	1.34%	2.67%	2.00%	**0.00%**
Wine	1.66%	26.73%	26.98%	12.25%	0.55%	0.54%	2.24%	1.68%	3.33%	0.54%	**0.00%**	1.83%
Heart	3.71%	25.93%	28.52%	15.56%	2.60%	3.34%	11.11%	4.45%	10.00%	3.71%	2.60%	**0.00%**
Parkinson's	17.78%	15.76%	3.51%	5.59%	16.40%	5.50%	12.14%	4.48%	8.52%	16.27%	4.89%	**0.00%**
Australian	7.64%	22.99%	19.80%	6.61%	6.91%	7.34%	4.88%	4.59%	8.79%	7.19%	6.60%	**0.00%**
Accumulate	32.77%	97.39%	80.13%	44.66%	28.44%	18.70%	33.69%	19.18%	31.96%	30.36%	16.07%	**1.83%**

one dataset, namely, the Australian, the proposed CECC-WDMSIF is superior to the CECR-MSIF. The average classification accuracy on the five UCI datasets of Table 7 for the proposed CECC-WDMSIF is 85.57±3.23%, which slightly outperforms the 84.15±4.88% from the CECR-MSIF.

To further compare the relative performance of the proposed CECC-WDMSIF and the CECR-MSIF, the differences between Max, Min, Avg and Std of each method and those of the best performing method are calculated for each dataset. Then, we accumulate these differences over five UCI datasets to evaluate the relative performance of the CECC-WDMSIF and CECR-MSIF. As shown in Table 9, for the proposed CECC-WDMSIF, the total accumulated difference across the five UCI datasets of Table 7 and the Max, Min, Avg and Std of accuracy of all classes is only 0.67%, yet the total accumulated difference showing 58.60% from the CECR-MSIF. Accordingly, the total difference in the best performance of the proposed CECC-WDMSIF is approximately 87.08 times less than that of the CECR-MSIF. It is thus concluded that the proposed CECC-WDMSIF outperforms the CECR-MSIF overall.

By analyzing the algorithms of CECR-MSIF and the proposed CECC-WDMSIF, it is learned that both of them leverage the fusion of CECR in CET for uncertainty reasoning. The reason why the performance of the proposed CECC-WDMSIF is superior to the CECR-MSIF is that the proposed CECC-WDMSIF takes advantage of CECC to manage conflicting CBBA effectively. As a result, the influence of conflicting CBBA is mitigated in the process of fusion by using CECC-WDMSIF.

6.2 Comparison

To validate the effectiveness of the proposed CECC-WDMSIF, we also compare it with several well-known related works, including the following eight state-of-the-art classifiers: Naïve Bayes (NaB) [57]; nearest mean classifier (NMC) [58]; k-nearest neighbor (kNN) [59]; Decision Tree (REPTree) [60]; support vector machine (SVM) [61]; SVM with radial basis function (SVM-RBF) [61]; multilayer perceptron (MlP) [62]; and RBF network (RBFN) [63]. We also compare it with the following three evidence theory-based fusion methods: k-nearest neighbor DS theory (kNN-DST) [64]; normal distribution-based classifier (NDC) [65]; and evidential calibration (EvC) [66]. Here, we compare the best performance of the CECC-WDMSIF with the above-mentioned methods.

As a comparative method, a five-fold cross validation is implemented as discussed in Section 6.1. The results of the classification accuracy and standard deviation generated by the different methods are shown in Table 10, in which the best performance is highlighted in bold. For all but one dataset, namely, Wine, the proposed CECC-WDMSIF is superior to the other well-known methods. The average classification accuracy on the five UCI datasets of Table 7 for the NaB, NMC, kNN, REPTree, SVM, SVM-RBF, MlP, RBFN, kNN-DST, NDC and EvC methods are 84.22%±10%, 71.29%±10.45%, 74.74%±13.07%, 81.84%±6.90%, 85.08%±9.73%, 87.03%±7.13%, 84.03%±8.71%, 86.93%±5.91%, 84.38%±8.38%, 84.70%±9.63% and 87.56%± 6.95%. The proposed CECC-WDMSIF has an average classification accuracy of 90.41%±4.6%, which is higher than that of other well-known related methods. This result demonstrates that the outcomes of the proposed CECC-WDMSIF have the highest classification accuracy and robustness on real-world datasets compared to eleven well-known related methods.

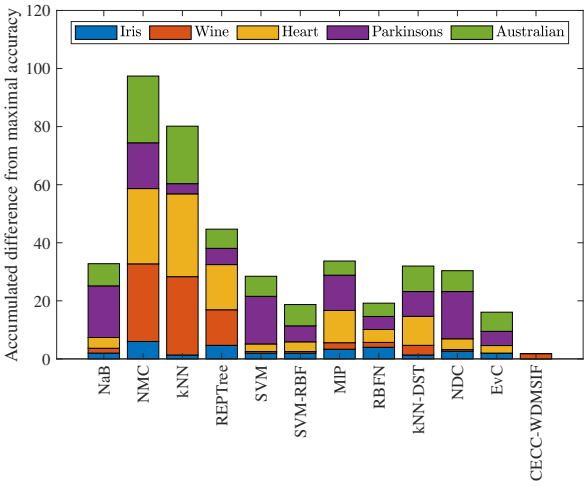

Fig. 6. Comparison of the accumulated difference between the accuracy and the maximal accuracy for different methods under several datasets in Section 6.2.

To better demonstrate the effectiveness of the proposed CECC-WDMSIF, for each dataset, the difference between the accuracy of each method and that of the best performing method is calculated as shown in Table 11. Then, the differences over five datasets are accumulated to evaluate the relative performance of each method. For the best case of the CECC-WDMSIF, the total accumulated difference across the five datasets is only 1.83%. As shown in Fig. 6, compared to the other methods, the total difference from the best performance for the CECC-WDMSIF is approximately 8.79 times smaller than the suboptimal method of EvC.

TABLE 12
Summarized information of the experimental datasets in Section 6.3.

Dataset	#Sample	#Class	#Attribute	Missing Value
Connectionist Bench	990	11	10	NO
Ecoli	336	8	7	NO
Breasttissue	101	6	10	NO
Pageblocks	5472	5	10	NO
Knowledge	403	4	5	NO

6.3 Extension of experiments

By analyzing CECC-WDMSIF algorithm in previous section, we notice that its complexity increases exponentially with the increase of the elements of the frame of discernment due to the CBBA generation method. It is considered that pairwise learning can decompose C_n-classes classification problem to $\frac{C_n(C_n-1)}{2}$ binary classification problems to improve the processing efficiency of the algorithm. Therefore, the CBBA generation method in Section 6.1 is integrated with pairwise learning [67] to produce CBBAs here.

TABLE 13
Comparison of the classification accuracy and standard deviations generated by different methods in Section 6.3.

Dataset	Classifiers								Evidence theory-based MSIF			
	NaB	NMC	kNN	REPTree	SVM	SVM-RBF	MIP	RBFN	kNN-DST	NDC	EvC	CECC-WDMSIF
Connectionist Bench	67.68%	99.09%	65.45%	88.48%	68.18%	80.40%	83.64%	94.42%	43.13%	76.33%	76.33%	**100.00%**
Ecoli	85.12%	84.94%	80.95%	83.93%	75.60%	42.56%	86.01%	**94.94%**	82.26%	52.77%	81.07%	92.63%
Breasttissue	61.32%	48.11%	50.00%	53.77%	46.23%	46.23%	50.00%	60.38%	61.43%	62.47%	55.43%	**100.00%**
Pageblocks	91.36%	29.96%	95.93%	**96.75%**	91.19%	89.80%	95.87%	94.25%	95.56%	85.79%	93.04%	95.81%
Knowledge	84.62%	74.94%	79.65%	88.34%	80.89%	32.01%	91.81%	90.07%	82.49%	72.66%	90.66%	**100.00%**
Avg	78.02%	67.41%	74.40%	82.25%	72.42%	58.20%	81.47%	86.81%	72.97%	70.00%	79.31%	**97.69%**
Std	11.47%	25.07%	15.55%	14.83%	15.09%	22.65%	16.31%	13.33%	18.50%	11.40%	13.41%	**3.00%**

TABLE 14
Comparison of the difference between the accuracy and standard deviation and the maximal accuracy and minimal standard deviations for eleven different methods under several datasets in Section 6.3.

Dataset	Classifiers								Evidence theory-based MSIF			
	NaB	NMC	kNN	REPTree	SVM	SVM-RBF	MIP	RBFN	kNN-DST	NDC	EvC	CECC-WDMSIF
Connectionist Bench	32.32%	0.91%	34.55%	11.52%	31.82%	19.60%	16.36%	5.58%	56.87%	23.67%	23.67%	**0.00%**
Ecoli	9.82%	10.00%	13.99%	11.01%	19.35%	52.38%	8.93%	**0.00%**	12.68%	42.17%	13.87%	2.31%
Breasttissue	38.68%	51.89%	50.00%	46.23%	53.77%	53.77%	50.00%	39.62%	38.57%	37.53%	44.57%	**0.00%**
Pageblocks	5.39%	66.79%	0.82%	**0.00%**	5.56%	6.94%	0.88%	2.50%	1.19%	10.96%	3.71%	0.94%
Knowledge	15.38%	25.06%	20.35%	11.66%	19.11%	67.99%	8.19%	9.93%	17.51%	27.34%	9.34%	**0.00%**
Accumulate	101.60%	154.65%	119.70%	80.42%	129.60%	200.68%	84.36%	57.62%	126.82%	141.67%	95.15%	**3.25%**

After that, we utilize CECC-WDMSIF algorithm to combine these CBBAs generated from multi-attribute of training samples in terms of different datasets. In this content, the computational complexity of the proposed CECC-WDMSIF algorithm decreases to $O(sn^2)$.

In this section, we compare the proposed CECC-WDMSIF algorithm with those well-known related work discussed in Section 6.2 based on datasets of Table 12 with 4, 5, 6, 8 and 11 classes. A five-fold cross validation is also implemented as the same as in Section 6.2. Through implementing different methods, the results of the classification accuracy and standard deviation are shown in Table 13, where the best performance is highlighted in bold. For datasets of Connectionist Bench, Breasttissue and Knowledge (http://archive.ics.uci.edu/ml/), the proposed CECC-WDMSIF outperforms the other well-known methods. The average classification accuracy on the five UCI datasets of Table 12 for the NaB, NMC, kNN, REPTree, SVM, SVM-RBF, MIP, RBFN, kNN-DST, NDC and EvC methods are 78.02%±11.47%, 67.41%±25.07%, 74.40%±15.55%, 82.25%±14.83%, 72.42%±15.09%, 58.20%±22.65%, 81.47%±16.31%, 86.81%±13.33%, 72.97%±18.50%, 70.00%±11.40% and 79.31%±13.41%. The proposed CECC-WDMSIF has an average classification accuracy of 97.69%±3.00%, which is higher than that of other well-known related methods.

To further illustrate the superiority of the proposed CECC-WDMSIF, the difference between the accuracy of each method and that of the best performing method for each datasets of Table 12 is calculated in Table 14. Next, the differences over all datasets of Table 12 are accumulated to assess the relative performance of each method. It is obvious that the best case is the CECC-WDMSIF, in which the total accumulated difference across the five datasets is only 3.25%; the worst case is the SVM-RBF, where the total accumulated difference across the five datasets is up to 200.68%. Compared to the other methods as shown in Fig. 7, the total difference from the best performance for the

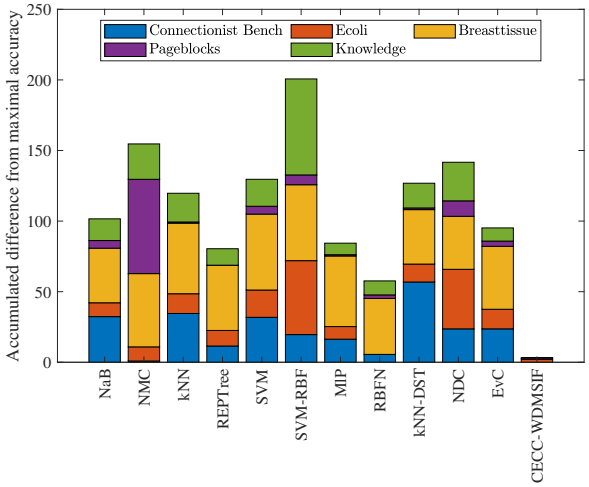

Fig. 7. Comparison of the accumulated difference between the accuracy and the maximal accuracy for different methods under five datasets in Section 6.3.

CECC-WDMSIF is approximately 17.74 times smaller than the suboptimal method of RBFN.

6.4 Discussion

From the above comparisons and evaluations, it is concluded that the proposed CECC-WDMSIF has the highest classification accuracy and robustness on real-world datasets. The dominant reasons are that 1) the proposed CECC can efficiently measure the correlation coefficients between CBBAs, so that the CECC-WDMSIF can manage conflict in the process of fusion effectively; 2) CECC-WDMSIF has an inherent advantage in solving missing value problems by taking advantage of CET framework; 3) CECC-WDMSIF reduces the influence of dataset noise on the decision-making system by fusing discounted complex evidences. Consequently, these merits of the proposed CECC-WDMSIF contribute to a higher decision level.

Although the proposed CECC-WDMSIF is effective to solve the pattern classification problem, its computational complexity depends on the cardinality of the frame of discernment in terms of generated CBBAs. A potential solution to mitigate this issue is deploying quantum information processing technology to CECC-WDMSIF to make our proposed CECC-WDMSIF more capable of handling complex and real-word application problems.

7 Conclusions

In this paper, a CECC was proposed to measure the correlation coefficient in complex evidence theory. Additionally, the CECC's properties—namely, nonnegativity, nondegeneracy, symmetry and boundedness—were defined and analyzed. Furthermore, a complex conflict coefficient was proposed in complex evidence theory. It was proven that the complex conflict coefficient had nonnegativity, symmetry, boundedness, extreme consistency, and insensitivity to refinement properties for conflict measurement. Moreover, several numerical examples demonstrated the superiority of the proposed complex conflict coefficient through comparisons. Finally, a weighted discounting multisource information fusion algorithm, called the CECC-WDMSIF, was designed based on the CECC to improve the performance of CET-based expert systems. By applying the proposed CECC-WDMSIF to the pattern classification of real-world datasets, it was demonstrated that the proposed CECC-WDMSIF had an advantage for diverse datasets and was more effective than the other well-known related methods.

The primary contribution of this article is that it is the first work to study the correlation and conflict coefficients between complex mass functions in CET. The complex correlation and conflict coefficients are generalized models for not only real numbers but also complex numbers. Therefore, the corresponding CECC-WDMSIF provides a promising way for uncertainty reasoning in expert systems, which has broad application prospects.

Conflict of Interest

The author states that there are no conflicts of interest.

Acknowledgments

The authors greatly appreciate the reviewers' suggestions and the editor's encouragement. This research is supported by the National Natural Science Foundation of China (No. 62003280) and Chongqing Talents: Exceptional Young Talents Project (cstc2022ycjh-bgzxm0070). In addition, this study is partially supported by Dr. Cao's ARC DECRA Fellowship DE220100265.

References

[1] I. Hatzilygeroudis and J. Prentzas, "Integrated rule-based learning and inference," *IEEE Transactions on Knowledge and Data Engineering*, vol. 22, no. 11, pp. 1549–1562, 2010.

[2] Q. Zhu, X. Zhou, J. Tan, and L. Guo, "Knowledge base reasoning with convolutional-based recurrent neural networks," *IEEE Transactions on Knowledge and Data Engineering*, vol. 33, no. 5, pp. 2015–2028, 2021.

[3] M. Zhou, M. Hu, Y.-W. Chen, B.-Y. Cheng, J. Wu, and E. Herrera-Viedma, "Towards achieving consistent opinion fusion in group decision making with complete distributed preference relations," *Knowledge-Based Systems*, vol. 236, p. 107740, 2022.

[4] D. Xie, F. Xiao, and W. Pedrycz, "Information quality for intuitionistic fuzzy values with its application in decision making," *Engineering Applications of Artificial Intelligence*, p. DOI: 10.1016/j.engappai.2021.104568, 2021.

[5] R. R. Yager, "Generalized Dempster–Shafer structures," *IEEE Transactions on Fuzzy Systems*, vol. 27, no. 3, pp. 428–435, 2019.

[6] Y. Tian, L. Liu, X. Mi, and B. Kang, "ZSLF: A new soft likelihood function based on Z-numbers and its application in expert decision system," *IEEE Transactions on Fuzzy Systems*, p. DOI: 10.1109/TFUZZ.2020.2997328, 2020.

[7] H.-C. Liu, X. Luan, Z. Li, and J. Wu, "Linguistic Petri nets based on cloud model theory for knowledge representation and reasoning," *IEEE Transactions on Knowledge and Data Engineering*, vol. 30, no. 4, pp. 717–728, 2018.

[8] A. P. Dempster, "Upper and lower probabilities induced by a multivalued mapping," *Annals of Mathematical Statistics*, vol. 38, no. 2, pp. 325–339, 1967.

[9] G. Shafer *et al.*, *A mathematical theory of evidence*. Princeton University Press Princeton, 1976, vol. 1.

[10] S. Destercke, P. Buche, and B. Charnomordic, "Evaluating data reliability: an evidential answer with application to a web-enabled data warehouse," *IEEE Transactions on Knowledge and Data Engineering*, vol. 25, no. 1, pp. 92–105, 2013.

[11] Z. Wang, C. Wang, X. Li, C. Gao, X. Li, and J. Zhu, "Evolutionary markov dynamics for network community detection," *IEEE Transactions on Knowledge and Data Engineering*, pp. 1–1, 2020.

[12] Z. Wang, Z. Li, R. Wang, F. Nie, and X. Li, "Large graph clustering with simultaneous spectral embedding and discretization," *IEEE Transactions on Pattern Analysis and Machine Intelligence*, vol. 43, no. 12, pp. 4426–4440, 2021.

[13] L. Chang, L. Zhang, C. Fu, and Y.-W. Chen, "Transparent digital twin for output control using belief rule base," *IEEE Transactions on Cybernetics*, p. DOI: 10.1109/TCYB.2021.3063285, 2021.

[14] C.-D. Wang, J.-H. Lai, and S. Y. Philip, "Multi-view clustering based on belief propagation," *IEEE Transactions on Knowledge and Data Engineering*, vol. 28, no. 4, pp. 1007–1021, 2015.

[15] Y.-T. Liu, N. R. Pal, A. R. Marathe, and C.-T. Lin, "Weighted fuzzy Dempster–Shafer framework for multimodal information integration," *IEEE Transactions on Fuzzy Systems*, vol. 26, no. 1, pp. 338–352, 2018.

[16] T. Denoeux, "Maximum likelihood estimation from uncertain data in the belief function framework," *IEEE Transactions on Knowledge and Data Engineering*, vol. 25, no. 1, pp. 119–130, 2013.

[17] Y. Song, J. Zhu, L. Lei, and X. Wang, "A self-adaptive combination method for temporal evidence based on negotiation strategy," *SCIENCE CHINA Information Sciences*, vol. 63, p. 210204, 2020.

[18] H. Fujita and Y.-C. Ko, "A heuristic representation learning based on evidential memberships: Case study of UCI-SPECTF," *International Journal of Approximate Reasoning*, vol. 120, 2020.

[19] Z. Liu, Y. Liu, J. Dezert, and F. Cuzzolin, "Evidence combination based on credal belief redistribution for pattern classification," *IEEE Transactions on Fuzzy Systems*, vol. 28, no. 4, pp. 618–631, 2020.

[20] X. Xu, J. Zheng, J.-b. Yang, D.-l. Xu, and Y.-w. Chen, "Data classification using evidence reasoning rule," *Knowledge-Based Systems*, vol. 116, pp. 144–151, 2017.

[21] A. Calzada, J. Liu, H. Wang, and A. Kashyap, "A new dynamic rule activation method for extended belief rule-based systems," *IEEE Transactions on knowledge and data engineering*, vol. 27, no. 4, pp. 880–894, 2014.

[22] C. Fu, M. Xue, W. Chang, D. Xu, and S. Yang, "An evidential reasoning approach based on risk attitude and criterion reliability," *Knowledge-Based Systems*, vol. 199, p. 105947, 2020.

[23] D. Ramot, R. Milo, M. Friedman, and A. Kandel, "Complex fuzzy sets," *IEEE Transactions on Fuzzy Systems*, vol. 10, no. 2, pp. 171–186, 2002.

[24] D. Ramot, M. Friedman, G. Langholz, and A. Kandel, "Complex fuzzy logic," *IEEE Transactions on Fuzzy Systems*, vol. 11, no. 4, pp. 450–461, 2003.

[25] H. Garg and D. Rani, "A robust correlation coefficient measure of complex intuitionistic fuzzy sets and their applications in decision-making," *Applied Intelligence*, vol. 49, no. 2, pp. 496–512, 2019.

[26] K. Ullah, T. Mahmood, Z. Ali, and N. Jan, "On some distance measures of complex Pythagorean fuzzy sets and their applications in pattern recognition," *Complex & Intelligent Systems*, pp. 1–13, 2019.

[27] F. Xiao, J. Wen, and W. Pedrycz, "Generalized divergence-based decision making method with an application to pattern classification," *IEEE Transactions on Knowledge and Data Engineering*, p. DOI: 10.1109/TKDE.2022.3177896, 2022.

[28] F. Xiao and W. Pedrycz, "Negation of the quantum mass function for multisource quantum information fusion with its application to pattern classification," *IEEE Transactions on Pattern Analysis and Machine Intelligence*, p. DOI: 10.1109/TPAMI.2022.3167045, 2022.

[29] J. W. Lai and K. H. Cheong, "Parrondo effect in quantum coin-toss simulations," *Physical Review E*, vol. 101, no. 5, p. 052212, 2020.

[30] F. Xiao, "Generalization of Dempster–Shafer theory: A complex mass function," *Applied Intelligence*, vol. 50, no. 10, pp. 3266–3275, 2019.

[31] ——, "Generalized belief function in complex evidence theory," *Journal of Intelligent & Fuzzy Systems*, vol. 38, no. 4, pp. 3665–3673, 2020.

[32] A.-L. Jousselme, D. Grenier, and É. Bossé, "A new distance between two bodies of evidence," *Information Fusion*, vol. 2, no. 2, pp. 91–101, 2001.

[33] C. Cheng and F. Xiao, "A distance for belief functions of orderable set," *Pattern Recognition Letters*, vol. 145, pp. 165–170, 2021.

[34] D. Han, J. Dezert, and Y. Yang, "Belief interval-based distance measures in the theory of belief functions," *IEEE Transactions on Systems, Man, and Cybernetics: Systems*, vol. 48, no. 6, pp. 833–850, 2016.

[35] D. Li, Y. Deng, and K. H. Cheong, "Multisource basic probability assignment fusion based on information quality," *International Journal of Intelligent Systems*, vol. 36, no. 4, pp. 1851–1875, 2021.

[36] X. Song and F. Xiao, "Combining time-series evidence: A complex network model based on a visibility graph and belief entropy," *Applied Intelligence*, pp. DOI: 10.1007/s10 489–021–02 956–5, 2022.

[37] L. Zhang and F. Xiao, "A novel belief $\chi 2$ divergence for multisource information fusion and its application in pattern classification," *International Journal of Intelligent Systems*, p. DOI: 10.1002/int.22912, 2022.

[38] C. Zhu, F. Xiao, and Z. Cao, "A generalized Rényi divergence for multi-source information fusion with its application in EEG data analysis," *Information Sciences*, p. DOI: 10.1016/j.ins.2022.05.012, 2022.

[39] L. Chen, Y. Deng, and K. H. Cheong, "Probability transformation of mass function: A weighted network method based on the ordered visibility graph," *Engineering Applications of Artificial Intelligence*, vol. 105, p. 104438, 2021.

[40] L. Xiong, X. Su, and H. Qian, "Conflicting evidence combination from the perspective of networks," *Information Sciences*, vol. 580, pp. 408–418, 2021.

[41] Q. Shang, H. Li, Y. Deng, and K. H. Cheong, "Compound credibility for conflicting evidence combination: an autoencoder-K-Means approach," *IEEE Transactions on Systems, Man, and Cybernetics: Systems*, p. 10.1109/TSMC.2021.3130187, 2021.

[42] W. Jiang, "A correlation coefficient for belief functions," *International Journal of Approximate Reasoning*, vol. 103, pp. 94–106, 2018.

[43] F. Xiao, "CED: A distance for complex mass functions," *IEEE Transactions on Neural Networks and Learning Systems*, vol. 32, no. 4, pp. 1525–1535, 2021.

[44] Y. Li, J. Chen, and L. Feng, "Dealing with uncertainty: A survey of theories and practices," *IEEE Transactions on Knowledge and Data Engineering*, vol. 25, no. 11, pp. 2463–2482, 2013.

[45] C. G. Akcora, Y. R. Gel, M. Kantarcioglu, V. Lyubchich,

and B. Thuraisingham, "Graphboot: Quantifying uncertainty in node feature learning on large networks," *IEEE Transactions on Knowledge and Data Engineering*, vol. 33, no. 1, pp. 116–127, 2019.

[46] Y. Deng, "Uncertainty measure in evidence theory," *SCIENCE CHINA Information Sciences*, vol. 63, no. 11, p. 210201, 2020.

[47] X. Deng and Y. Cui, "An improved belief structure satisfaction to uncertain target values by considering the overlapping degree between events," *Information Sciences*, vol. 580, pp. 398–407, 2021.

[48] C. Qiang, Y. Deng, and K. H. Cheong, "Information fractal dimension of mass function," *Fractals*, p. DOI: 10.1142/S0218348X22501109, 2022.

[49] Y. Deng, "Information volume of mass function," *International Journal of Computers Communications & Control*, vol. 15, no. 6, p. 3983, 2020.

[50] J. Deng and Y. Deng, "Information volume of fuzzy membership function," *International Journal of Computers Communications & Control*, vol. 16, no. 1, p. 4106, 2021.

[51] K. Zhan, C. Niu, C. Chen, F. Nie, C. Zhang, and Y. Yang, "Graph structure fusion for multiview clustering," *IEEE Transactions on Knowledge and Data Engineering*, vol. 31, no. 10, pp. 1984–1993, 2018.

[52] D. Smith and S. Singh, "Approaches to multisensor data fusion in target tracking: A survey," *IEEE Transactions On Knowledge and Data Engineering*, vol. 18, no. 12, pp. 1696–1710, 2006.

[53] Z. Cao, C.-H. Chuang, J.-K. King, and C.-T. Lin, "Multi-channel EEG recordings during a sustained-attention driving task," *Scientific Data*, vol. 6, pp. DOI: 10.1038/s41 597–019–0027–4, 2019.

[54] Q. Li, A. Alipour-Fanid, M. Slawski, Y. Ye, L. Wu, K. Zeng, and L. Zhao, "Large-scale cost-aware classification using feature computational dependency graph," *IEEE Transactions on Knowledge and Data Engineering*, vol. 33, no. 5, pp. 2029–2044, 2021.

[55] F. J. Valverde-Albacete and C. Peláez-Moreno, "A framework for supervised classification performance analysis with information-theoretic methods," *IEEE Transactions on Knowledge and Data Engineering*, vol. 32, no. 11, pp. 2075–2087, 2019.

[56] F. Xiao, "A new divergence measure for belief functions in D-S evidence theory for multisensor data fusion," *Information Sciences*, vol. 514, pp. 462–483, 2020.

[57] B.-G. Hu, "What are the differences between Bayesian classifiers and mutual-information classifiers?" *IEEE Transactions on Neural Networks and Learning Systems*, vol. 25, no. 2, pp. 249–264, 2013.

[58] C. J. Veenman and M. J. Reinders, "The nearest subclass classifier: A compromise between the nearest mean and nearest neighbor classifier," *IEEE Trans. Pattern Anal. Mach. Intell.*, vol. 27, no. 9, pp. 1417–1429, 2005.

[59] T. Cover and P. Hart, "Nearest neighbor pattern classification," *IEEE Transactions on Information Theory*, vol. 13, no. 1, pp. 21–27, 1967.

[60] Y. Freund and L. Mason, "The alternating decision tree learning algorithm," in *Int. Conf. Mach. Learn.*, vol. 99. Citeseer, 1999, pp. 124–133.

[61] C.-C. Chang and C.-J. Lin, "LIBSVM: a library for support vector machines," *ACM Transactions on Intelligent Systems and Technology*, vol. 2, no. 3, pp. 1–27, 2011.

[62] C. L. Castro and A. P. Braga, "Novel cost-sensitive approach to improve the multilayer perceptron performance on imbalanced data," *IEEE Transactions on Neural Networks and Learning Systems*, vol. 24, no. 6, pp. 888–899, 2013.

[63] S. Chen, C. F. Cowan, and P. M. Grant, "Orthogonal least squares learning algorithm for radial basis function networks," *IEEE Transactions on Neural Networks*, vol. 2, no. 2, pp. 302–309, 1991.

[64] T. Denœux, "A k-nearest neighbor classification rule based on Dempster–Shafer theory," *IEEE Transactions on Systems, Man, and Cybernetics*, vol. 25, no. 5, pp. 804–813, 1995.

[65] P. Xu, Y. Deng, X. Su, and S. Mahadevan, "A new method to determine basic probability assignment from training data," *Knowledge-Based Systems*, vol. 46, pp. 69–80, 2013.

[66] P. Xu, F. Davoine, H. Zha, and T. Denoeux, "Evidential calibration of binary SVM classifiers," *International Journal of Approximate Reasoning*, vol. 72, pp. 55–70, 2016.

[67] C. Zhu, B. Qin, F. Xiao, Z. Cao, and H. M. Pandey, "A fuzzy preference-based Dempster–Shafer evidence theory for decision fusion," *Information Sciences*, vol. 570, pp. 306–322, 2021.

[68] M. Bouchard, A.-L. Jousselme, and P.-E. Doré, "A proof for the positive definiteness of the jaccard index matrix," *International Journal of Approximate Reasoning*, vol. 54, no. 5, pp. 615–626, 2013.

[69] E. W. Weisstein, "Conjugate transpose," *https://mathworld. wolfram. com/*, 2003.

APPENDIX

Proof

Proof *(1) Considering two arbitrary CBBAs $\mathbb{M}_\mu$ and $\mathbb{M}_\nu$ in FOD $\mathbf{\Omega}$, we have*

$$\mathbb{C}(\mathbb{M}_\mu,\mathbb{M}_\nu)=\frac{\sqrt{\langle\overrightarrow{\mathbb{M}}_\mu,\overrightarrow{\mathbb{M}}_\nu\rangle\langle\overrightarrow{\mathbb{M}}_\nu,\overrightarrow{\mathbb{M}}_\mu\rangle}}{\|\overrightarrow{\mathbb{M}}_\mu\|\|\overrightarrow{\mathbb{M}}_\nu\|}.$$

Obviously, $\mathbb{C}(\mathbb{M}_\mu,\mathbb{M}_\nu)\geq 0$ can be conducted, which proves the nonnegativity property of the CECC.

(2) Considering two arbitrary CBBAs $\mathbb{M}_\mu=\mathbb{M}_\nu$ in FOD $\mathbf{\Omega}$ with hypotheses $\mathcal{A}_i$ and $\mathcal{A}_j$, we have

$$\begin{aligned}\mathbb{C}(\mathbb{M}_\mu,\mathbb{M}_\nu)&=\frac{\sqrt{\langle\overrightarrow{\mathbb{M}}_\mu,\overrightarrow{\mathbb{M}}_\mu\rangle\langle\overrightarrow{\mathbb{M}}_\mu,\overrightarrow{\mathbb{M}}_\mu\rangle}}{\|\overrightarrow{\mathbb{M}}_\mu\|\|\overrightarrow{\mathbb{M}}_\mu\|}\\&=\frac{\sqrt{\langle\overrightarrow{\mathbb{M}}_\nu,\overrightarrow{\mathbb{M}}_\nu\rangle\langle\overrightarrow{\mathbb{M}}_\nu,\overrightarrow{\mathbb{M}}_\nu\rangle}}{\|\overrightarrow{\mathbb{M}}_\nu\|\|\overrightarrow{\mathbb{M}}_\nu\|}=1.\end{aligned}$$

Conversely, considering $\mathbb{C}(\mathbb{M}_\mu,\mathbb{M}_\nu)=1$, we have

$$\frac{\sqrt{\langle\overrightarrow{\mathbb{M}}_\mu,\overrightarrow{\mathbb{M}}_\nu\rangle\langle\overrightarrow{\mathbb{M}}_\nu,\overrightarrow{\mathbb{M}}_\mu\rangle}}{\|\overrightarrow{\mathbb{M}}_\mu\|\|\overrightarrow{\mathbb{M}}_\nu\|}=1.$$

Then, we obtain

$$\begin{aligned}&\sum_{i=1}^{2^n-1}\sum_{j=1}^{2^n-1}\mathbb{M}_\mu(\mathcal{A}_i)\widehat{\mathbb{M}}_\nu(\mathcal{A}_j)\frac{|\mathcal{A}_i\cap\mathcal{A}_j|}{|\mathcal{A}_i\cup\mathcal{A}_j|}\cdot\\&\sum_{i=1}^{2^n-1}\sum_{j=1}^{2^n-1}\mathbb{M}_\nu(\mathcal{A}_j)\widehat{\mathbb{M}}_\mu(\mathcal{A}_i)\frac{|\mathcal{A}_j\cap\mathcal{A}_i|}{|\mathcal{A}_j\cup\mathcal{A}_i|}=\\&\sum_{i=1}^{2^n-1}\sum_{j=1}^{2^n-1}\mathbb{M}_\mu(\mathcal{A}_i)\widehat{\mathbb{M}}_\mu(\mathcal{A}_j)\frac{|\mathcal{A}_i\cap\mathcal{A}_j|}{|\mathcal{A}_i\cup\mathcal{A}_j|}\cdot\\&\sum_{i=1}^{2^n-1}\sum_{j=1}^{2^n-1}\mathbb{M}_\nu(\mathcal{A}_j)\widehat{\mathbb{M}}_\nu(\mathcal{A}_i)\frac{|\mathcal{A}_j\cap\mathcal{A}_i|}{|\mathcal{A}_j\cup\mathcal{A}_i|}.\end{aligned}$$

This equation is only satisfied for $1\leq i,j\leq 2^n$

$$\widehat{\mathbb{M}}_\mu(\mathcal{A}_i)=\widehat{\mathbb{M}}_\nu(\mathcal{A}_i)\quad and\quad \widehat{\mathbb{M}}_\mu(\mathcal{A}_j)=\widehat{\mathbb{M}}_\nu(\mathcal{A}_j),$$

such that

$$\mathbb{M}_\mu=\mathbb{M}_\nu.$$

Therefore, $\mathbb{C}(\mathbb{M}_\mu,\mathbb{M}_\nu)=1\Longleftrightarrow\mathbb{M}_\mu=\mathbb{M}_\nu$, which proves the nondegeneracy property of the CECC.

(3) Consider two arbitrary CBBAs $\mathbb{M}_\mu$ and $\mathbb{M}_\nu$ in FOD $\mathbf{\Omega}$ with hypotheses $\mathcal{A}_i$ and $\mathcal{A}_j$.

For $\langle\overrightarrow{\mathbb{M}}_\mu,\overrightarrow{\mathbb{M}}_\nu\rangle$, we have

$$\langle\overrightarrow{\mathbb{M}}_\mu,\overrightarrow{\mathbb{M}}_\nu\rangle=\sum_{i=1}^{2^n-1}\sum_{j=1}^{2^n-1}\mathbb{M}_\mu(\mathcal{A}_i)\widehat{\mathbb{M}}_\nu(\mathcal{A}_j)\frac{|\mathcal{A}_i\cap\mathcal{A}_j|}{|\mathcal{A}_i\cup\mathcal{A}_j|}.\tag{1A}$$

Additionally, for $\langle\overrightarrow{\mathbb{M}}_\nu,\overrightarrow{\mathbb{M}}_\mu\rangle$, we have

$$\langle\overrightarrow{\mathbb{M}}_\nu,\overrightarrow{\mathbb{M}}_\mu\rangle=\sum_{i=1}^{2^n-1}\sum_{j=1}^{2^n-1}\mathbb{M}_\nu(\mathcal{A}_j)\widehat{\mathbb{M}}_\mu(\mathcal{A}_i)\frac{|\mathcal{A}_j\cap\mathcal{A}_i|}{|\mathcal{A}_j\cup\mathcal{A}_i|}.\tag{2A}$$

From Eqs. (1A) and (2A), it is obvious that

$$\langle\overrightarrow{\mathbb{M}}_\mu,\overrightarrow{\mathbb{M}}_\nu\rangle\langle\overrightarrow{\mathbb{M}}_\nu,\overrightarrow{\mathbb{M}}_\mu\rangle=\langle\overrightarrow{\mathbb{M}}_\nu,\overrightarrow{\mathbb{M}}_\mu\rangle\langle\overrightarrow{\mathbb{M}}_\mu,\overrightarrow{\mathbb{M}}_\nu\rangle.$$

Since

$$\mathbb{C}(\mathbb{M}_\mu,\mathbb{M}_\nu)=\frac{\sqrt{\langle\overrightarrow{\mathbb{M}}_\mu,\overrightarrow{\mathbb{M}}_\nu\rangle\langle\overrightarrow{\mathbb{M}}_\nu,\overrightarrow{\mathbb{M}}_\mu\rangle}}{\|\overrightarrow{\mathbb{M}}_\mu\|\|\overrightarrow{\mathbb{M}}_\nu\|},$$

and

$$\mathbb{C}(\mathbb{M}_\nu,\mathbb{M}_\mu)=\frac{\sqrt{\langle\overrightarrow{\mathbb{M}}_\nu,\overrightarrow{\mathbb{M}}_\mu\rangle\langle\overrightarrow{\mathbb{M}}_\mu,\overrightarrow{\mathbb{M}}_\nu\rangle}}{\|\overrightarrow{\mathbb{M}}_\nu\|\|\overrightarrow{\mathbb{M}}_\mu\|},$$

it is easily concluded that

$$\mathbb{C}(\mathbb{M}_\mu,\mathbb{M}_\nu)=\mathbb{C}(\mathbb{M}_\nu,\mathbb{M}_\mu),$$

which proves the symmetry property of the CECC.

(4) Consider two arbitrary CBBAs $\mathbb{M}_\nu$ and $\mathbb{M}_\mu$ in FOD $\mathbf{\Omega}$.

Since D is a Hermitian positive-definite matrix [68], for a $2^n\times 2^n$ lower triangular matrix M, it can be as follows:

$$D=M^HM,$$

where H is the conjugate transpose [69].

Thus, from [42, 69], we have

$$\begin{aligned}\langle\overrightarrow{\mathbb{M}}_\mu,\overrightarrow{\mathbb{M}}_\mu\rangle&=p^HDp=p^HM^HMp;\\\langle\overrightarrow{\mathbb{M}}_\mu,\overrightarrow{\mathbb{M}}_\nu\rangle&=p^HDq=p^HM^HMq;\\\langle\overrightarrow{\mathbb{M}}_\nu,\overrightarrow{\mathbb{M}}_\mu\rangle&=q^HDp=q^HM^HMp;\\\langle\overrightarrow{\mathbb{M}}_\nu,\overrightarrow{\mathbb{M}}_\nu\rangle&=q^HDq=q^HM^HMq.\end{aligned}$$

Thus,

$$\mathbb{C}(\mathbb{M}_\mu,\mathbb{M}_\nu)=\frac{\sqrt{p^HM^HMq}\sqrt{q^HM^HMp}}{\sqrt{p^HM^HMp}\sqrt{q^HM^HMq}}.$$

Because $p^HM^HMp=(Mp)^H(Mp)=\|Mp\|^2$, by using the triangle inequality on the vector 2-norm [42, 69], we obtain

$$\begin{aligned}\|M(p+q)\|^2\leq(\|Mp\|+\|Mq\|)^2\Longrightarrow\\(p+q)^HM^HM(p+q)\leq(\sqrt{p^HM^HMp}+\sqrt{q^HM^HMq})^2\Longrightarrow\\p^HM^HMp+p^HM^HMq+q^HM^HMp+q^HM^HMq\leq\\p^HM^HMp+q^HM^HMq+2\sqrt{p^HM^HMpq^HM^HMq}\Longrightarrow\\p^HM^HMq+q^HM^HMp\leq 2\sqrt{p^HM^HMpq^HM^HMq}.\end{aligned}$$

Since $p^HM^HMq=(p^HM^HMq)^H=q^HM^HMp$ [42, 69], we obtain

$$\begin{aligned}\frac{p^HM^HMq}{\sqrt{p^HM^HMpq^HM^TMq}}\leq 1,\\\frac{q^HM^HMp}{\sqrt{p^HM^HMpq^HM^TMq}}\leq 1,\end{aligned}$$

so that

$$\frac{\sqrt{p^HM^HMq}\sqrt{q^HM^HMp}}{\sqrt{p^HM^HMp}\sqrt{q^HM^TMq}}\leq 1.$$

Therefore, as proven in (1), $\mathbb{C}(\mathbb{M}_\mu,\mathbb{M}_\nu)\geq 0$, which obtains

$$0\leq\mathbb{C}(\mathbb{M}_\mu,\mathbb{M}_\nu)\leq 1,$$

which proves the boundedness property of the CECC.

TABLE 1A
An example of constructed complex interval number models for Sepal length (SL) attribute.

Hypotheses	Attributes
	SL
$\mathbb{M}(\{Se\})$	[4.6724+0.3166i, 5.3927+0.3166i]
$\mathbb{M}(\{Ve\})$	[5.4316+0.3702i, 6.3351+0.3702i]
$\mathbb{M}(\{Vi\})$	[5.9806+0.4139i, 7.1784+0.4139i]
$\mathbb{M}(\{Se, Ve\})$	–
$\mathbb{M}(\{Se, Vi\})$	–
$\mathbb{M}(\{Ve, Vi\})$	[5.9806+0.4139i, 6.3351+0.3702i]
$\mathbb{M}(\{Se, Ve, Vi\})$	–

TABLE 2A
An example of constructed complex interval number models for Sepal width (SW) attribute.

Hypotheses	Attributes
	SW
$\mathbb{M}(\{Se\})$	[3.0421+0.2163i, 3.8343+0.2163i]
$\mathbb{M}(\{Ve\})$	[2.4333+0.1724i, 3.0459+0.1724i]
$\mathbb{M}(\{Vi\})$	[2.6541+0.1873i, 3.2992+0.1873i]
$\mathbb{M}(\{Se, Ve\})$	[3.0421+0.2163i, 3.0459+0.1724i]
$\mathbb{M}(\{Se, Vi\})$	[3.0421+0.2163i, 3.2992+0.1873i]
$\mathbb{M}(\{Ve, Vi\})$	[2.6541+0.1873i, 3.0459+0.1724i]
$\mathbb{M}(\{Se, Ve, Vi\})$	[3.0421+0.2163i, 3.0459+0.1724i]

TABLE 3A
An example of constructed complex interval number models for Petal length (PL) attribute.

Hypotheses	Attributes
	PL
$\mathbb{M}(\{Se\})$	[1.2773+0.0921i, 1.6519+0.0921i]
$\mathbb{M}(\{Ve\})$	[3.7565+0.2658i, 4.6918+0.2658i]
$\mathbb{M}(\{Vi\})$	[4.9534+0.3452i, 6.0199+0.3452i]
$\mathbb{M}(\{Se, Ve\})$	–
$\mathbb{M}(\{Se, Vi\})$	–
$\mathbb{M}(\{Ve, Vi\})$	–
$\mathbb{M}(\{Se, Ve, Vi\})$	–

Example

Here, we provide an example to illustrate CBBA generation in accordance with different attributes of a testing sample in terms of Iris dataset with three classes of Setosa (Se), Versicolor (Ve) and Virginica (Vi). Based on the selected training data from Iris dataset (http://archive.ics.uci.edu/ml/), the complex interval number models are constructed in accordance with four attributes of Sepal length (SL), Sepal width (SW), Petal length (PL) and Petal width (PW) as shown in Table 1A-Table 4A, respectively.

Next, taking a testing sample with four attributes of Setosa class as an instance: SL = 5.1 cm, SW = 3.8 cm, PL

TABLE 4A
An example of constructed complex interval number models for Petal width (PW) attribute.

Hypotheses	Attributes
	PW
$\mathbb{M}(\{Se\})$	[0.1363+0.0157i, 0.3627+0.0157i]
$\mathbb{M}(\{Ve\})$	[1.1059+0.0824i, 1.5140+0.0824i]
$\mathbb{M}(\{Vi\})$	[1.7444+0.1270i, 2.2926+0.1270i]
$\mathbb{M}(\{Se, Ve\})$	–
$\mathbb{M}(\{Se, Vi\})$	–
$\mathbb{M}(\{Ve, Vi\})$	–
$\mathbb{M}(\{Se, Ve, Vi\})$	–

TABLE 5A
CBBAs generated from Sepal length (SL) attribute of a testing sample in terms of Setosa class of Iris dataset.

Hypotheses	Attributes
	SL
$\mathbb{M}(\{Se\})$	0.9485-0.0007i
$\mathbb{M}(\{Ve\})$	0.0234+0.0003i
$\mathbb{M}(\{Vi\})$	0.0112+0.0001i
$\mathbb{M}(\{Se, Ve\})$	0
$\mathbb{M}(\{Se, Vi\})$	0
$\mathbb{M}(\{Ve, Vi\})$	0.0170+0.0003i
$\mathbb{M}(\{Se, Ve, Vi\})$	0

TABLE 6A
CBBAs generated from Sepal width (SW) attribute of a testing sample in terms of Setosa class of Iris dataset.

Hypotheses	Attributes
	SW
$\mathbb{M}(\{Se\})$	0.5596-0.0196i
$\mathbb{M}(\{Ve\})$	0.0342+0.0008i
$\mathbb{M}(\{Vi\})$	0.0562+0.0017i
$\mathbb{M}(\{Se, Ve\})$	0.0786+0.0034i
$\mathbb{M}(\{Se, Vi\})$	0.1494+0.0092i
$\mathbb{M}(\{Ve, Vi\})$	0.0433+0.0012i
$\mathbb{M}(\{Se, Ve, Vi\})$	0.0786+0.0034i

TABLE 7A
CBBAs generated from Petal length (PL) attribute of a testing sample in terms of Setosa class of Iris dataset.

Hypotheses	Attributes
	PL
$\mathbb{M}(\{Se\})$	0.9999+0.0047i
$\mathbb{M}(\{Ve\})$	-0.0273-0.0028i
$\mathbb{M}(\{Vi\})$	-0.0185-0.0019i
$\mathbb{M}(\{Se, Ve\})$	0
$\mathbb{M}(\{Se, Vi\})$	0
$\mathbb{M}(\{Ve, Vi\})$	0
$\mathbb{M}(\{Se, Ve, Vi\})$	0.0458+4.34E-19i

= 1.6 cm, PW = 0.2 cm. We utilize the CBBA generation method discussed in Section 6.1 to obtain four CBBAs in accordance with those four attributes as shown in Table 5A-Table 8A, respectively.

Then, by implementing the proposed CECC-WDMSIF algorithm, a fused CBBA is generated as shown in Table 9A. After that, the CBet values for hypotheses with singletons are calculated as shown in Table 10A. Finally, by calculating the absolute value of CBet, a predicted target is determined as shown in Table 11A.

TABLE 8A
CBBAs generated from Petal width (PW) attribute of a testing sample in terms of Setosa class of Iris dataset.

Hypotheses	Attributes
	PW
$\mathbb{M}(\{Se\})$	0.9997+0.0225i
$\mathbb{M}(\{Ve\})$	-0.1273-0.0146i
$\mathbb{M}(\{Vi\})$	-0.0719-0.0078i
$\mathbb{M}(\{Se, Ve\})$	0
$\mathbb{M}(\{Se, Vi\})$	0
$\mathbb{M}(\{Ve, Vi\})$	0
$\mathbb{M}(\{Se, Ve, Vi\})$	0.1995-3.47E-18i

TABLE 9A
Fused CBBA according to generated CBBAs in Table 5A-Table 8A.

Hypotheses	Fused CBBA
$\mathbb{M}(\{Se\})$	0.9999+8.50E-06i
$\mathbb{M}(\{Ve\})$	-1.07E-05-5.30E-06i
$\mathbb{M}(\{Vi\})$	9.62E-06-3.91E-06i
$\mathbb{M}(\{Se, Ve\})$	3.08E-07+7.77E-09i
$\mathbb{M}(\{Se, Vi\})$	5.85E-07+2.50E-08i
$\mathbb{M}(\{Ve, Vi\})$	2.40E-05+6.68E-07i
$\mathbb{M}(\{Se, Ve, Vi\})$	4.75E-07+4.68E-09i

TABLE 10A
CBet value for hypotheses with singletons according to the fused CBBA in Table 9A.

Hypotheses	CBet
$\mathbb{M}(\{Se\})$	0.9999+8.52E-06i
$\mathbb{M}(\{Ve\})$	1.59E-06-4.96E-06i
$\mathbb{M}(\{Vi\})$	2.21E-05-3.56E-06i
$\mathbb{M}(\{Se, Ve\})$	–
$\mathbb{M}(\{Se, Vi\})$	–
$\mathbb{M}(\{Ve, Vi\})$	–
$\mathbb{M}(\{Se, Ve, Vi\})$	–

TABLE 11A
Predicted target according to |CBet|.

Hypotheses	|CBet|	Predicted target
$\mathbb{M}(\{Se\})$	0.9999	✓
$\mathbb{M}(\{Ve\})$	5.21E-06	✗
$\mathbb{M}(\{Vi\})$	2.24E-05	✗
$\mathbb{M}(\{Se, Ve\})$	–	–
$\mathbb{M}(\{Se, Vi\})$	–	–
$\mathbb{M}(\{Ve, Vi\})$	–	–
$\mathbb{M}(\{Se, Ve, Vi\})$	–	–

TABLE 12A
Classification accuracy and standard deviation generated by the CECR-MSIF and CECC-WDMSIF under θ variation.

	Accuracy	Iris		Wine		Heart		Parkinson's		Australian	
		CECR-MSIF	CECC-WDMSIF	CECR-MSIF	CECC-WDMSIF	CECR-MSIF	CECC-WDMSIF	CECR-MSIF	CECC-WDMSIF	CECR-MSIF	CECC-WDMSIF
Class 1	Max	100.0%	100.0%	96.61%	96.61%	98.67%	94.67%	83.33%	79.17%	93.21%	94.52%
	Min	100.0%	100.0%	72.88%	83.05%	87.33%	88.00%	6.25%	12.50%	68.93%	85.38%
	Avg	100.0%	100.0%	90.40%	91.76%	92.93%	91.73%	58.91%	54.78%	84.14%	92.85%
	Std	0.00%	0.00%	6.09%	5.09%	2.37%	1.95%	24.39%	21.10%	5.85%	2.18%
Class 2	Max	98.00%	98.00%	95.77%	94.37%	73.33%	77.50%	98.64%	97.96%	92.51%	83.06%
	Min	78.00%	80.00%	66.20%	78.87%	40.00%	59.17%	58.50%	70.07%	79.80%	70.68%
	Avg	89.14%	92.94%	81.63%	85.03%	65.57%	73.30%	83.65%	86.83%	87.86%	75.38%
	Std	5.96%	4.90%	7.77%	4.41%	7.23%	4.02%	9.14%	6.77%	3.74%	2.81%
Class 3	Max	92.00%	92.00%	100.0%	100.0%	–	–	–	–	–	–
	Min	76.00%	80.00%	93.75%	95.83%	–	–	–	–	–	–
	Avg	87.33%	87.33%	99.31%	99.47%	–	–	–	–	–	–
	Std	4.22%	4.20%	1.47%	1.08%	–	–	–	–	–	–
All classes	Max	96.67%	96.67%	94.94%	93.82%	83.70%	85.93%	82.56%	83.08%	87.54%	86.52%
	Min	86.67%	90.00%	80.90%	86.52%	72.59%	78.89%	50.26%	61.54%	78.84%	83.62%
	Avg	92.16%	93.42%	89.30%	91.15%	80.77%	83.54%	77.56%	78.94%	85.80%	85.08%
	Std	2.88%	1.94%	3.81%	2.09%	2.58%	1.31%	7.03%	4.64%	2.14%	0.64%

TABLE 13A
Comparison of the differences between the accuracy and standard deviation and the maximal accuracy and minimal standard deviations for two different methods under several datasets.

Accuracy (All classes)	Iris		Wine		Heart		Parkinson's		Australian		ACC	
	CECR-MSIF	CECC-WDMSIF	CECR-MSIF	CECC-WDMSIF	CECR-MSIF	CECC-WDMSIF	CECR-MSIF	CECC-WDMSIF	CECR-MSIF	CECC-WDMSIF	CECR-MSIF	CECC-WDMSIF
Max	0.00%	0.00%	0.00%	1.12%	2.22%	0.00%	0.51%	0.00%	0.00%	1.01%	2.74%	2.14%
Min	3.33%	0.00%	5.62%	0.00%	6.30%	0.00%	11.28%	0.00%	4.78%	0.00%	31.31%	0.00%
Avg	1.27%	0.00%	1.85%	0.00%	2.77%	0.00%	1.39%	0.00%	0.00%	0.72%	7.27%	0.72%
Std	0.94%	0.00%	1.71%	0.00%	1.27%	0.00%	2.38%	0.00%	1.50%	0.00%	7.80%	0.00%
ACC	5.54%	**0.00**%	9.18%	**1.12**%	12.56%	**0.00**%	15.57%	**0.00**%	6.28%	**1.73**%	49.12%	**2.86**%